T.R.
GEBZE TECHNICAL UNIVERSITY
GRADUATE SCHOOL

DUCT DESIGN OF RECIPROCATING ENGINE COOLING SYSTEM AT AIRCRAFT WHICH HAS TRACTOR CONFIGURATION

RİFAT RAMİZ AYDIN

A THESIS OF MASTER OF SCIENCE
DEPARTMENT OF ENERGY TECHNOLOGIES IN APPLIED PROPULSION SYSTEM DESIGN & ENGINEERING FOR AEROSPACE TECHNOLOGIES PROGRAM

ADVISOR: PROF. DR. MEHMET ALİ ARSLAN

JULY 2024

T.R.

GEBZE TECHNICAL UNIVERSITY

GRADUATE SCHOOL

DUCT DESIGN OF RECIPROCATING ENGINE COOLING SYSTEM AT AIRCRAFT WHICH HAS TRACTOR CONFIGURATION

RİFAT RAMİZ AYDIN

A THESIS OF MASTER OF SCIENCE

DEPARTMENT OF ENERGY TECHNOLOGIES IN APPLIED PROPULSION SYSTEM DESIGN & ENGINEERING FOR AEROSPACE TECHNOLOGIES PROGRAM

ADVISOR: PROF. DR. MEHMET ALİ ARSLAN

JULY 2024

T.C.
GEBZE TEKNİK ÜNİVERSİTESİ
LİSANSÜSTÜ EĞİTİM ENSTİTÜSÜ

ÇEKİCİ KONFİGÜRASYONUNA SAHİP HAVA ARACINDAKİ PİSTONLU MOTORUN SOĞUTMA SİSTEMİNİN HAVA ALIĞI TASARIMI

RİFAT RAMİZ AYDIN

YÜKSEK LİSANS TEZİ
ENERJİ TEKNOLOJİLERİ ANABİLİM DALI
HAVACILIK VE UZAY TEKNOLOJİLERİNDE UYGULAMALI İTKİ SİSTEMİ TASARIM MÜHENDİSLİĞİ PROGRAMI

DANIŞMAN: PROF. DR. MEHMET ALİ ARSLAN

TEMMUZ 2024

MASTER of SCIENCE JURY APPROVAL FORM

A thesis submitted by Rifat Ramiz AYDIN, defended on 10/07/2024 before the jury formed with the 08/07/2024 date and 2024/35 numbered decision of the GTU Graduate Administration Board, has been accepted as a MASTER of SCIENCE thesis in the Department of Energy Technologies, Applied Propulsion System Design & Engineering for Aerospace Technologies Program.

JURY

MEMBER
(THESIS ADVISOR): Prof. Dr. Mehmet Ali ARSLAN

MEMBER: Dr.Öğr.Üyesi Mahmut Akşit

MEMBER: Prof. Dr. Gökhan Bayar

APPROVAL

Gebze Technical University Graduate Administration Board
/ / date and / numbered decision.

SIGNATURE/SEAL

ABSTRACT

This paper explores the design, challenges, and solutions related to cooling duct systems for four-stroke reciprocating engines in aircraft. The reliability and efficiency of these engines are crucial, as they are a popular choice due to their balance of power and efficiency. Effective engine cooling is essential to prevent overheating, which can lead to engine failure, reduced performance, and increased maintenance costs. The cooling system design must manage thermal loads efficiently while minimizing additional weight and aerodynamic drag.

This paper delves into the principles of cooling duct design, considering factors such as aerodynamic efficiency, material selection, and integration with the overall aircraft design. A case study is presented, showcasing the cooling duct design for an aircraft powered by a twin turbocharged engine. The design process involves using Computational Fluid Dynamics (CFD) analysis to simulate airflow and optimize duct performance. Additionally, the paper covers the implementation and testing of a prototype cooling duct, demonstrating significant improvements in temperature regulation and overall engine performance.

The study concludes with a summary of findings and implications for future aircraft designs, emphasizing the importance CFD in optimizing cooling systems. This research provides valuable insights for engineers and researchers aiming to enhance cooling performance of aircraft that powered by reciprocating engine and operational efficiency through improved cooling duct design.

Key Words: Cooling Systems, 4-Stroke Reciprocating Engines, Computational Fluid Dynamics (CFD), Aircraft Duct Design, Engine Thermal Management

ÖZET

Bu tezde 4 zamanlı pistonlu motor kullanan hava aracının soğutma sistemi bileşenleri için gerekli olan soğutma alığının tasarımı ve analiz çalışmasını içermektedir. 4 zamanlı pistonlu motorlar güvenilirlik ve verimlilik açısından hava araçları için revaçta olan motorlardır. Motor performans düşüşü, bakım maliyetlerinin artışı ve aşırı ısınma kaynaklı motor arızalarının önlemek için etkin bir motor soğutma çözümü uygulamak önemlidir. Hava araçlarında soğutma sistemi tasarımı motor kaynaklı termal yükleri başarılı şekilde idare ederken, hava aracına minimum ağırlık artışı ve soğutma sistemi kaynaklı sürtünme etkisi getirmelidir. Soğutma sistemi tasarımın doğru şekilde yapılması, ek ağırlığı ve aerodinamik direnci en aza indirirken ısıl yükleri verimli bir şekilde yönetilmesi açısından önem taşımaktadır.

Bu tez, aerodinamik verimlilik, malzeme seçimi ve genel uçak tasarımıyla entegrasyon gibi faktörleri göz önünde bulundurarak soğutma kanalı tasarımının prensiplerini ele almaktadır. Çift turboşarjlı bir motorla çalışan bir uçak için soğutma kanalı tasarımını gösteren bir vaka çalışması sunulmaktadır. Tasarım süreci, hava akışını simüle etmek ve kanal performansını optimize etmek için Hesaplamalı Akışkanlar Dinamiği (CFD) analizinin kullanımını içermektedir. Ayrıca, tez bir prototip soğutma kanalının uygulanmasını ve test edilmesini kapsamaktadır ve sıcaklık düzenlemesinde ve genel motor performansında önemli iyileştirmeler göstermektedir.

Çalışma, CFD'nin soğutma sistemlerini optimize etmedeki önemini vurgulayarak, gelecekteki uçak tasarımları için bulguların ve çıkarımların bir özetini sunmaktadır. Bu araştırma, piston motor kullanan hava aracının soğutma performansını ve operasyonel verimliliği geliştirmek amacıyla, mühendisler ve araştırmacılar için değerli bilgiler sağlamaktadır.

Anahtar Kelimeler: Soğutma Sistemleri, 4 Zamanlı Pistonlu Motorlar, Hesaplamalı Akışkanlar Dinamiği (CFD), Hava Alığı Tasarımı, Motor Termal Yönetimi

ACKNOWLEDGEMENTS

I would like to express my deepest gratitude to everyone who contributed to the realization of this thesis.

First and foremost, I am deeply indebted to my esteemed advisor, Prof. Dr. Mehmet Ali Arslan, for his continuous support, guidance, and encouragement. His knowledge and experience have played a significant role in shaping this study.

I owe a great debt of gratitude to my family, who have always been by my side, providing me with endless love and support. They have been my greatest source of motivation throughout this journey.

I would like to extend my sincere thanks to İbrahim Ethem Kazancı and Kemal Buğra Avşar for their meaningful friendship and assistance. This journey would not have been conclude without their support.

My heartfelt thanks go to Fulya Erdemir for her academic and moral support. Her contributions and ideas have greatly enriched this study.

I am grateful to Berke Gök for his valuable assistance. His help has significantly contributed to the development of this work.

To everyone who contributed to the successful completion of this thesis, I express my deepest gratitude.

TABLE OF CONTENTS

	Page
ABSTRACT	v
ÖZET	vi
ACKNOWLEDGEMENTS	vii
TABLE OF CONTENTS	viii
LIST OF SYMBOLS AND ABBREVIATIONS	ix
LIST OF FIGURES	x
LIST OF TABLES	xii
1. INTRODUCTION	1
2. LITERATURE SURVEY	12
3. METODS AND MATERIALS	17
3.1. Requirement Definition	18
3.2. Preliminary Design	23
3.3. Analysis	32
4. RESULT AND DISCUSSION	40
5. CONCLUSION AND FUTURE WORK	52
REFERENCES	53
BIOGRAPHY	56
PUBLICATION AND PRESENTATIONS FROM THE THESIS	57

LIST OF SYMBOLS AND ABBREVIATIONS

A	: Area
ρ	: Density
D	: Diameter
y+	: Dimensionless wall distance
Φ	: Dissipation function
s	: Entropy
q	: Heat flux vector
i	: Internal Energy
L	: Length
Q	: Mass flow rate
p	: Pressure
Δp	: Pressure drop
τ	: Shear stress
C_v	: Specific heat
υ	: Specific volume
T	: Temperature
t	: Time
R	: Universal gas constant
V	: Velocity
abs	: Absolute pressure
CRDID	: Common rail direct injection diesel
CFD	: Computational fluid dynamic
CAD	: Computer aided design
DFVAs	: Ducted fan aerial vehicles
ECS	: Environmental control system
ECU	: Engine control unit
FADEC	: Full authority digital engine control
HVAC	: Heating ventilation and air conditioning
ICE	: Internal combustion engine
ISA	: International standard atmosphere
TVD	: Torsional vibration damper
UAV	: Unmanned aerial vehicle
VTOL	: Vertical take-off and landing

LIST OF FIGURES

Page

Figure 1.1: p-υ and T-s diagrams of the ideal Diesel cycle [1]. 2
Figure 1.2: p-υ and T-s diagrams of the ideal Otto cycle [1]. 2
Figure 1.3: Illustration of cooling airflow belongs to air cooled engine [2]. 3
Figure 1.4: Aircraft Using Air-Cooled Engines [3-8]. 4
Figure 1.5: Illustration of cooling system belongs to liquid cooled engine [9]. 7
Figure 1.6: Propeller Slipstream [10]. 11
Figure 2.1: A simple ducted radiator design [36]. 15
Figure 2.2: A simple ducted radiator design [36]. 15
Figure 3.1: Overview of configuration 1. 24
Figure 3.2: Detailed view of intercooler1-duct pair at configuration 1 a) left view, b) trimetric view from left, c) trimetric view from right, d) cross section view. 25
Figure 3.3: Centre of areas a) inlet, b) exit. 25
Figure 3.4: Detailed view of intercooler2-duct pair at configuration 1 a) left view, b) trimetric view from left, c) trimetric view from right, d) cross section view. 26
Figure 3.5: Centre of areas a) inlet, b) exit. 26
Figure 3.6: Detailed view of radiator core and duct couple at configuration 1 a) left view, b) trimetric view from left, c) trimetric view from right, d) cross section view. 27
Figure 3.7: Centre of areas a) inlet, b) exit. 27
Figure 3.8: Centre of areas a) inlet, b) exit. 28
Figure 3.9: Overview of configuration 2. 28
Figure 3.10: Detailed view of intercooler1-duct pair at configuration 2 a) left view, b) trimetric view from left, c) trimetric view from right, d) cross section view. 29
Figure 3.11: Centre of areas a) inlet, b) exit. 29
Figure 3.12: Detailed view of intercooler2-duct pair at configuration 2 a) left view, b) trimetric view from left, c) trimetric view from right, d) cross section view. 30
Figure 3.13: Centre of areas a) inlet, b) exit. 30
Figure 3.14: Detailed view of radiator core and duct couple at configuration 2 a) left view, b) trimetric view from left, c) trimetric view from right, d) cross section view. 31
Figure 3.15: Centre of areas a) inlet, b) exit. 31
Figure 3.16: Cross sectional view of radiator, intercooler 1 and intercooler 2 ducts a) intercooler 1 ducts, b) intercooler 2 ducts, c) radiator ducts. 32
Figure 3.17: Stress components on three faces of fluid element [41]. 34
Figure 3.18: Surface mesh of aircraft fuselage. 38
Figure 3.19: Volume mesh of inspected space. 38
Figure 3.20: Detail view of volume mesh. 39
Figure 4.1: Velocity profile of ducts at inlet. 41
Figure 4.2: Cross sectional view of radiator duct at bisector plane. 42
Figure 4.3: Velocity profile at the exit of radiator. 42
Figure 4.4: Velocity profile at the exit of intercooler 1. 43
Figure 4.5: Velocity profile at the exit of intercooler 2. 43
Figure 4.6: Turbocharger 1 inlet temperature versus time. 46
Figure 4.7: Turbocharger 1 outlet temperature versus time. 46
Figure 4.8: Intercooler 1 outlet temperature versus time. 47
Figure 4.9: Turbocharger 2 outlet temperature versus time. 47
Figure 4.10: Manifold temperature versus time. 48
Figure 4.11: Coolant temperature versus time 48

Figure 4.12: Auxiliary flight parameters a) barometric pressure b) load lever input (throttle position). 49
Figure 4.13: Manifold temperature at early phase of climbing and take-off. 50
Figure 4.14 Coolant temperature at early phase of climbing and take-off. 51

LIST OF TABLES

	Page
Table 3.1: Radiator requirements.	19
Table 3.2: Intercooler-1 requirements.	19
Table 3.3: Intercooler-2 requirements.	20
Table 3.4: Radiator specification.	21
Table 3.5: Intercooler 1 specification.	22
Table 3.6: Intercooler 2 specification.	22
Table 4.1: Radiator thermal performance.	40
Table 4.2: Intercooler 1 thermal performance.	40
Table 4.3: Intercooler 2 thermal performance.	41
Table 4.4: Mechanical properties of ULTEM AM9085F.	44

1. INTRODUCTION

Based on the location and function of the engine or propeller in terms of the direction of flight, aircraft are mostly classified as pusher or tractor types. The engines and propellers of pusher-type aircraft are positioned toward the back of the aircraft, pushing it through the air instead of pulling it. The engines and propellers of a tractor-type aircraft are positioned at the front of the aircraft to pull it through the air. Since the early 20th century, tractor-type layout has been the most widely used in aviation.

A reciprocating engine, also known as a piston engine, is a heat engine that utilizes one or more reciprocating pistons to convert pressure into a rotating motion. This type of engine is one of the most common forms of internal combustion engines (ICE) and is widely used in various applications, including automobiles, aircraft, and other machinery.

Internal combustion engines operate through a sequence of strokes that admit and remove gases to and from the cylinder. These operations are repeated cyclically and an engine is said to be Two-stroke or Four-stroke depending on the number of strokes it takes to complete a cycle. Two-Stroke engine completes a power cycle in just two strokes of the piston (one compression stroke and one exhaust stroke) and one revolution of the crankshaft. Four-Stroke engine completes a power cycle in four strokes of the piston (intake, compression, power, and exhaust) and two revolutions of the crankshaft.

Diesel Cycle and Otto Cycle are the most common thermodynamic cycles that empower the four-stroke reciprocating engines. According to the cycle employed by the engine, ignition is accomplished by either a spark plug or an increased temperature of compressed air inside of the cylinder. Gasoline engines generate power through the Otto Cycle as well as diesel engines obey the steps of the Diesel Cycle.

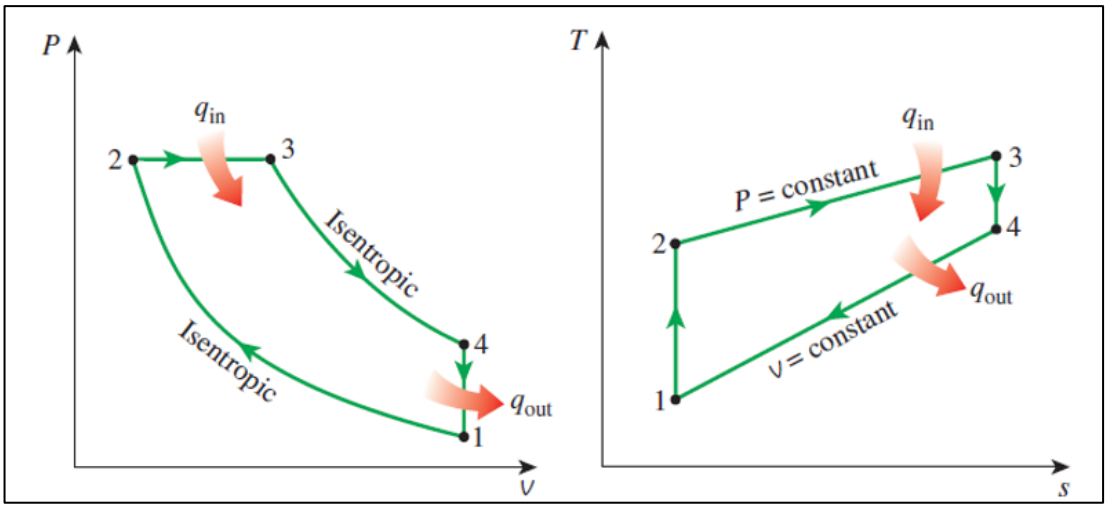

Figure 1.1: p-υ and T-s diagrams of the ideal Diesel cycle [1].

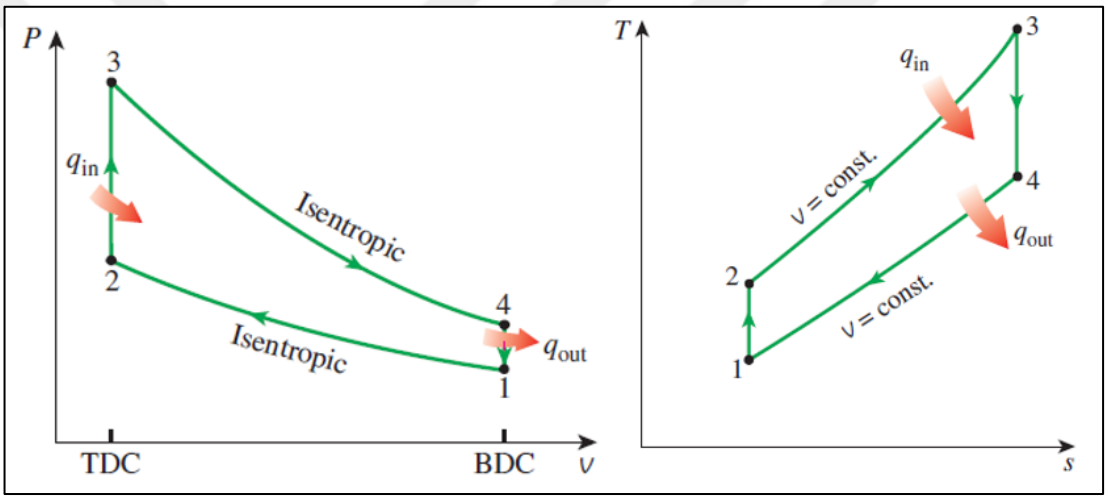

Figure 1.2: p-υ and T-s diagrams of the ideal Otto cycle [1].

Reciprocating engines generate a lot of heat due to the combustion of fuel and the friction of moving parts. If this heat is not effectively managed, it can lead to engine inefficiency, decreased performance, and even engine failure. To deal with these issues, engines require cooling system to regulate the engine's temperature. The heat that needs to be dissipated from the engine is generally transferred to a fluid, ensuring that the engine operates under optimum conditions. Engine cooling systems are divided into two classes depending on the type of fluid that draws heat. The two primary types of cooling systems are air-cooled and liquid-cooled. Each system has its unique characteristics and applications.

Air-cooled engines dissipate heat directly into the air without the use of a liquid coolant. This is achieved by using fins attached to the engine block and cylinder head,

which increase the surface area exposed to the air. As the engine operates, air flows over these fins and absorbs the heat from the engine.

In air-cooled engines, fins are an inherent element of the cylinder head and block. These fins expand the surface area exposed to the cooling air, allowing for more efficient heat transmission from the engine to the air. The greater surface area supplied by the fins enables quick heat dissipation into the surrounding air. Shrouding or cowling is utilized to direct airflow toward the fins. This improves the cooling effect by directing air directly onto hot surfaces. The shrouding controls the direction and flow of air, ensuring that all sections of the engine receive proper cooling. In some air-cooled engines, especially those in aircraft, cooling ducts are used to channel air to the hottest parts of the engine. Some air-cooled engines, particularly those in aircraft, employ cooling ducts to direct air to the engine's hottest sections. These ducts assist manage airflow more accurately, ensuring that even the most thermally stressed components receive enough cooling.

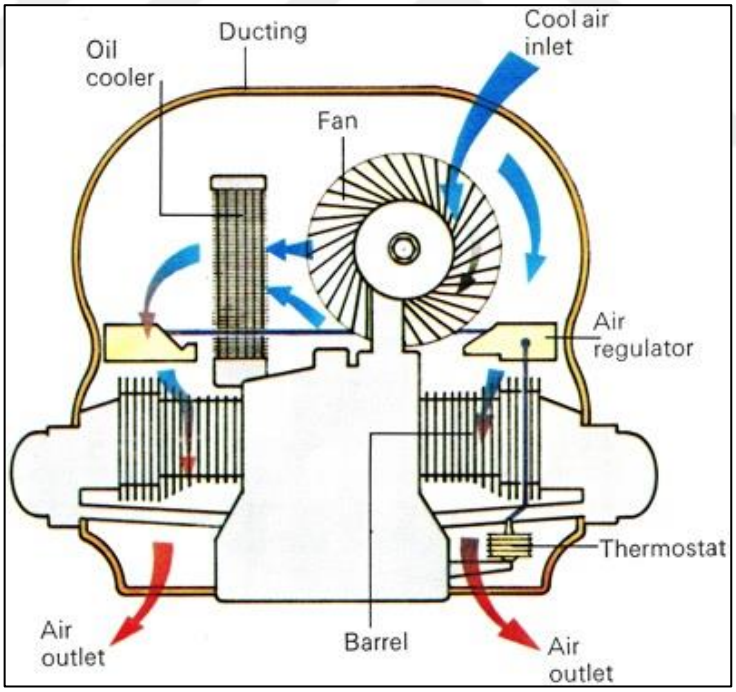

Figure 1.3: Illustration of cooling airflow belongs to air cooled engine [2].

Cessna 172

Piper PA-28 Cherokee

Beechcraft Bonanza

Cirrus SR22

Vans RV Serisi

Focke-Wulf Fw 190

Figure 1.4: Aircraft Using Air-Cooled Engines [3-8].

Air-cooled engines are commonly used in motorcycles, small portable generators, and small aircraft where weight and simplicity are more critical than precise temperature control. It has fewer components than liquid-cooled engines like radiators, hoses, or water pump. Since it has fewer parts, its maintainability and reliability are high. However, it is not effective in managing heat under high load conditions or in stationary applications. Since this system uses free or conditioned air flowing through the engine, cooling starts from the engine surface. Hence, hot spots form in the inner parts of the engine. This reduces the temperature control over the engine. Also, it is

not as effective in managing heat under high load conditions or in stationary applications (**Figure 1.4**).

Examining **Figure 1.4** [3-8]:

- Cessna 172: One of the most produced civil aircraft in the world, equipped with air-cooled engines like the Lycoming O-320.
- Piper PA-28 Cherokee: Widely used in general aviation, this aircraft is powered by air-cooled engines such as the Lycoming O-360.
- Beechcraft Bonanza: This light aircraft is equipped with air-cooled engines like the Continental IO-550.
- Cirrus SR22: This popular general aviation aircraft uses the Continental IO-550 air-cooled engine.
- Vans RV Series: These kit planes are typically equipped with air-cooled engines such as the Lycoming O-360 or similar.
- Focke-Wulf Fw 190: Used by the German Luftwaffe during World War II, this fighter aircraft was powered by the BMW 801 air-cooled radial engine.

To absorb and release heat, liquid-cooled engines need a coolant mixture, which is usually water-based plus additions like glycol. Heat is absorbed by the coolant as it moves through channels in the engine block and heads. Before returning to the engine block, it is circulated via a radiator and emits heat into the atmosphere. The circulation is completed when the coolant that exits the radiator returns to the engine block. The liquid coolant continually circulates through the engine block, absorbs heat, and carries it away to the radiator. Heat is absorbed by the liquid coolant, which moves back and forth continuously between the engines block and the radiator.

Liquid-cooled engines have four fundamental components: coolant, radiator, water pump, and thermostat. Coolant is a water-based solution containing antifreeze (ethylene glycol) or a comparable substance. The radiator dissipates heat that is absorbed by coolant from the engine into the atmosphere. Continuous fluid circulation through the system is provided by water pump driven by TVD of engine. The thermostat regulates coolant flow based on temperature, ensuring that the engine heats up instantly and operates at a steady temperature.

The cooling ability of a liquid-cooled engine depends on several system parts and parameters. Every modification may have a unique impact on the overall performance of the engine, including power output, durability, and efficiency.

The cooling capacity can be improved by utilizing a more efficient core design or by enlarging the radiator. Heat can be dispersed more efficiently via high-efficiency radiators with more fins per inch or advanced materials like aluminium. Nevertheless, bulkier or more sophisticated radiators may need more room and add weight, which could have an impact on the vehicle's weight distribution or aerodynamics. The coolant flow rate can be increased by using a water pump with a larger capacity or by improving the efficiency of the current pump. Increased flow rate improves the amount of coolant that circulates through the engine in a given amount of time providing a better heat transfer rate and effectively cooling the engine. Increased flow rates could demand greater power to operate the pump, so marginally diminishing engine efficiency. Furthermore, excessively high flow rates can decrease the cooling time that coolant flows through the inner passage of the radiator and leave it for heat absorption, which might negatively impact cooling efficiency. Enhancing heat transfer and lowering scaling and corrosion in the cooling system can be achieved by using a coolant with higher thermal conductivity and specific heat capacity. Enhancing heat transfer and lowering scaling and corrosion in the cooling system can be achieved by using a coolant with higher thermal conductivity and specific heat capacity. Most high-performance coolants with high thermal conductivity may cost more and need more frequent changes or particular maintenance techniques. The coolant may start to circulate through the radiator sooner if the thermostat is adjusted to a lower temperature. Fuel efficiency and pollutants are reduced as the engine reaches its ideal operating temperature faster and is maintained more consistently. A too-early thermostat opening could lengthen the engine's warm-up process and marginally lower efficiency during that time. Enhancing cooling performance can also be achieved by strategically placing the radiator and designing the ducting to maximize air intake and minimize hot air from the engine being recirculated. By doing this, the radiator is guaranteed to receive the coolest air possible, maximizing its heat-dissipating performance. Nevertheless, this strategy might necessitate a considerable reworking of the nacelle's shape and interior arrangement. If the decision is made at a point where

the design phase concludes and manufacturing begins, the cost of the product drastically could be increased.

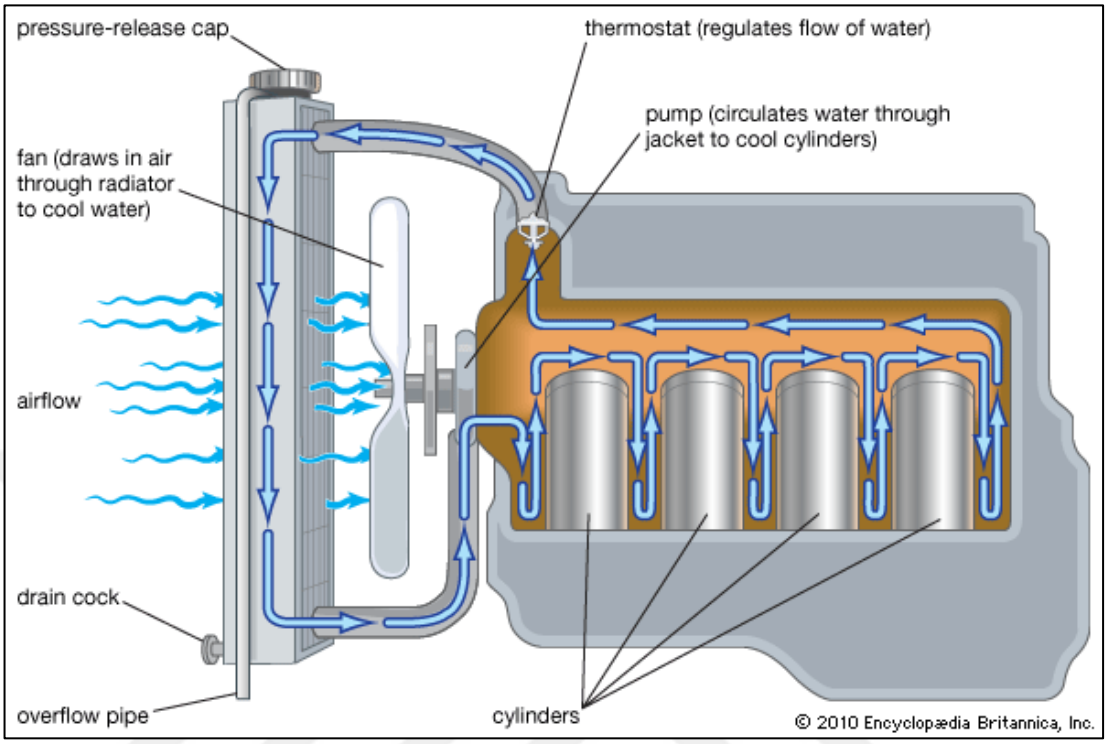

Figure 1.5: of cooling system belongs to liquid cooled engine [9].

For larger or more complex engines where exact temperature control is essential, liquid cooling is recommended. Hence liquid-cooled engines are frequently used in automotive, aviation and marine applications. Liquid cooled systems offers great flexibility to differentiate cooling capacity by arranging the radiator size or regulate coolant flow by adjusting water pump.

On the other hand, liquid-cooled engines are more complex than their counterparts. Components such as radiator, coolant, water pump and hoses could potentially fail. Also, each component has its own weight, and the coolant amount adds additional weight to the overall weight of the engine. The chemical structure of coolant degrades by time and renewal of coolant is mandatory. Sometimes hose of the cooling system can get brittle due to continuous exposure to thermal gradients or inconvenient coolant usage. In the end, maintenance costs are inevitable.

The placement of cooling components creates unique challenges and opportunities. Placement in aerodynamically sensitive areas requires carefully designed ducting that

channels air efficiently without disrupting the airflow around the aircraft. If components are placed in a less optimal position for aerodynamics, more sophisticated ducting might be needed to route air effectively, which can increase drag. The positioning of components should minimize interference with the nose's aerodynamic profile. This often means integrating them into the fuselage's existing lines and making sure that all air intakes and outlets are made to preserve smooth airflow. The positioning also needs to consider the effects of heat on various parts. For instance, hot air shouldn't be circulated back and forth between the intercooler and radiator. To lessen this, use thermal barriers or adequate space. Maintenance is another issue that mostly do not pay attention to while components are placed inside of fuselage. It should be simple to reach the components for maintenance. Their positioning of access panels and other nose structural components is impacted by this factor.

The radiator is commonly placed directly behind the engine and ahead of the firewall in airplanes with engines located at the nose. In this position, the radiator can take advantage of the propeller's cool air stream, which offers a steady airflow that is essential for efficient heat dissipation. Depending on the available space and the fuselage's design, the radiator is often angled to face the incoming airflow, which can be either vertical or horizontal. A larger surface area may be possible with horizontal positioning, but more intricate ductwork may be needed to properly conduct airflow over the whole surface.

To optimize its cooling efficiency, the intercooler for turbocharged engines, which cools the air compressed by the turbocharger, is also positioned in the airflow stream. It is usually located close to the radiator but far enough away to prevent heat transfer. Intercoolers can be positioned above, besides, or below the radiator, depending on the design specifications and available space. This way, they can get enough air without getting in the way of the radiator's flow.

According to placement of components rough shape of ducts stars to appear. Following the installation of the intercooler and radiator inside the nose, intake ducts are carefully designed to maximize airflow while minimizing drag. Usually placed directly behind or below the propeller, these ducts are designed to take advantage of the high-pressure area at the front of the nose. Controlling the hot air outflow from the intercooler and radiator is essential. Heated air must be directed by exhaust ducts out of the aircraft and away from critical parts without interfering with engine or other temperature-

sensitive equipment operation. The heated air is typically vented via the fuselage's bottom or sides to accomplish this.

The purpose of ducts is to effectively direct airflow from the aircraft's exterior to its interior cooling systems. To ensure that the system functions well in all flying situations, the duct must supply a sufficient amount of air to the cooling components (such as radiators or intercoolers) or to any area that needs ventilation. This involves drawing air in through carefully positioned intakes and distributing it across the radiator and intercooler surfaces, where it is most required. Without the need for extra mechanical parts like fans, efficient ducting uses the dynamic pressure of air flowing at high speeds to boost the flow rate of the cooling system. This is especially significant for high-performance aircraft, where it's critical to maintain ideal engine and system temperatures throughout a range of operating conditions. Engines produce large amounts of heat, and they can overheat if proper cooling is not provided. This can result in decreased engine longevity, reduced efficiency, or even engine failure. Ensuring efficient cooling keeps the engine running in a temperature range that maximizes power production and fuel efficiency while reducing pollutants and wear. The smooth flow of air over the aircraft's body could otherwise be disrupted by the layout of external components like intercoolers and radiators, which ducts help to streamline. Ducting aids in preserving the engine's optimum temperature conditions by regulating the volume and speed of airflow. Aside from considering altitude and speed, effective duct design also considers other flight variables that can have significant effects on the internal and exterior pressures and, in turn, the cooling dynamics. Smooth internal surfaces in ducts lower turbulence and friction. Curves should avoid sharp bends and have a large radius of curvature in order to maintain airflow speed and prevent pressure loss. To decrease the length of the ducts and lower potential energy losses and pressure drops, the routing should be as direct as possible.

Several kinds of aerodynamic drag in aircraft can be caused by cooling systems and the ducting that surrounds them. A disruption in the laminar flow of air over the aircraft's surface can increase form drag and cause turbulence if the air inlets and outlets for cooling systems are not carefully planned or positioned. Form drag can be considerably increased by large, projecting intakes or poorly designed exhaust vents. Friction drag is caused by the friction between the surface of the duct and the air flowing over it. Rough or corrugated duct surfaces can elevate friction drag compared

to smoother surfaces. The drag produced by airflow through the cooling system, which includes radiators, intercoolers, and related ducts, is referred to as cooling drag, which is a subset of friction drag that is unique to cooling systems. Air passing through a radiator encounters resistance due to the fins and channels designed to maximize heat transfer, thereby increasing drag.

Cooling duct design is greatly impacted by the propeller when an engine with a propeller is mounted at the front of the aircraft fuselage. The way cooling systems, especially the ducting, are built is largely dependent on how the propeller affects the airflow dynamics surrounding the aircraft. In aircraft aerodynamics, the propeller slipstream effect is quite important, particularly when it comes to cooling system effectiveness for aircraft with propeller-driven engines (**Figure 1.6**). A column of accelerated and twisted air behind the propeller, created by the propeller's rotation, is known as the slipstream. Depending on the layout of the aircraft, this accelerated air forms a cylinder-shaped flow pattern that encircles a portion of the fuselage and sometimes the wings behind the propeller. The higher air velocity in the slipstream greatly improves the heat transfer coefficient because air moving more quickly can transfer more heat away from the surface more effectively. To optimize the amount of air directed through the cooling system, cooling duct air intakes can be positioned inside the slipstream. This arrangement guarantees that even in situations where the aircraft is traveling slowly or is fixed on the ground, the cooling components will always have access to air. It's critical to control the hot air exhaust from the cooling system properly. The hot air exhaust vents have to be positioned so as not to interfere with the propeller's airflow, prevent hot air from recirculating into the cooling system, and protect other temperature-sensitive parts.

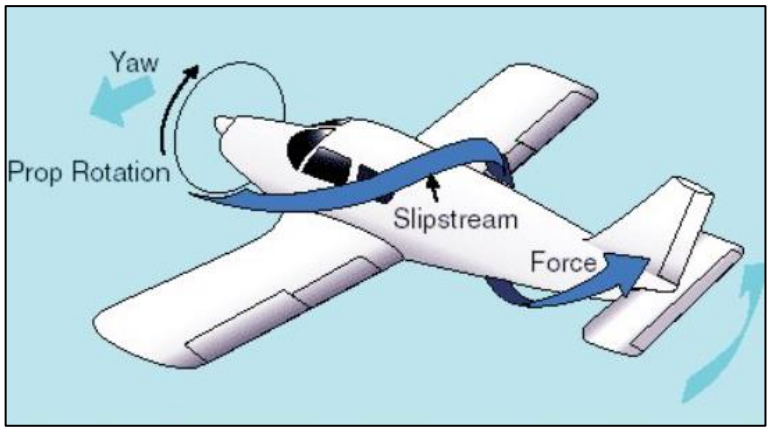

Figure 1.6: Propeller Slipstream [10].

This study will describe how to design air ducts to deliver the cooling air required by the cooling system components of the engine of a tractor-type configuration aircraft powered by a four-stroke, liquid-cooled, twin-turbocharged engine. For this purpose, each component, including the radiator and intercoolers, will have two air ducts. After the radiators and intercoolers, which are the main components of the cooling system, are placed in the fuselage to meet the airflow as perpendicularly as possible to the remaining space from the engine and support equipment, the air duct design phase, which is the main subject of the study, will commence. Air ducts have been designed to be as streamlined as possible to avoid a pressure drop while transferring the flow rate demanded by the cooling system components. The air duct that transfers the required flow rate along the allowable pressure drop limit to ensure enough heat dissipation for components will be investigated by computational fluid dynamics software. The best possible design will be tested in the aircraft, and the analytical results will be compared to the test data. If the cooling system achieves the expected heat rejection at take-off when the engine's thermal demand is highest, the designed air ducts will be regarded as successful, and the work will be completed.

2. LITERATURE SURVEY

Liquid-cooled aircraft engines are often perceived with a certain allure and fascination that air-cooled engines lack. This perception is partly due to the aesthetic appeal of liquid-cooled engines, which are associated with streamlined, aerodynamically efficient designs. Such engines evoke images of iconic aircraft like the Spitfire, Mustang, and Messerschmitt, which contribute to their legendary status. In contrast, radial air-cooled engines do not share this aesthetic advantage and are generally seen as less visually appealing. Similarly, modern horizontally-opposed air-cooled engines do not garner the same enthusiasm. The concept of liquid-cooling tends to inspire designers to envision low-drag shapes and enhanced performance, while marketers are drawn to striking visuals like lightning-bolt and shark-mouth paint schemes. Nevertheless, when evaluated against more objective criteria, air-cooled engines demonstrate favourable comparisons to liquid-cooled engines [11]. This subject has been studied extensively from the past to the present.

CRDID (Common Rail Direct Injection Diesel) engines were developed in the automobile industry and have extensive testing data. Millions of devices have been manufactured, and trillions of hours of dependability data are available. These engines can also run on jet fuel, and a combination of the two fuels can be obtained by tuning the ECU map appropriately, removing the requirement for airport refuelling. In their study, Luca et al. studied the potential advantages of the use of CRDID engines transferred from automotive to aviation and the development of a special cooling solution for these engines. Simulations on medium-sized helicopters, such as the Eurocopter EC 120, have shown that the pressure difference between the intake and exhaust sites is remarkably constant under all flight situations [12]. CRDID engines face challenges of both overcooling and overheating. Maintaining optimal temperatures of the cylinder head, piston, and liner is crucial for combustion efficiency. Extended idling periods, especially in tropical climates, can lead to overcooling due to the engine's high efficiency even at low loads. Overcooling causes increased clearance between liners and piston rings, leading to blow-by contamination of fuel into the lubricant and increased liner wear. Controlling maximum temperatures is vital for engine durability; exceeding these limits can rapidly lead to failures such as increased blow-by, reduced power output, and accelerated lubricant consumption,

and eventual major failures like piston or exhaust valve failures [13-17]. Coolant temperature regulation is typically managed by a liquid-to-liquid heat exchanger, using a thermostatic valve or variable velocity coolant pump. Automotive engines, due to emissions regulations, require rapid heating after cold starts, aided by cooling accessories like generators. Overcooling is effectively controlled in helicopter applications through precise monitoring and control by FADEC (Full Authority Digital Engine Control). Conversely, managing heating involves efficient heat dissipation across all flight phases. While fans are an option, they have limitations and are not effective during critical flight conditions like Take Off, Hover-1, and Hover-2, where maximum power is required without significant airflow from the main rotor [18-21]. Efficient cooling duct design, particularly inlet and outlet positioning, is critical for helicopters. Effective heating relies on adequate forced airflow, particularly challenging in conditions with minimal rotor-induced velocity [22,23].

Vertical Take-Off and Landing (VTOL) aerial vehicles have sparked significant interest in both academia and industry over the last few years. VTOL aircraft, such as Ducted Fan Aerial Vehicles (DFAVs), do not require runways and may operate in confined, hazardous, and cluttered environments since their propellers are covered by a duct, unlike rotary-wing aerial vehicles [24]. In addition, their thrust vectoring capacity makes them more suited than standard Unmanned Aerial Vehicle (UAV) setups. Nevertheless, these airborne vehicles have a slightly more sophisticated aerodynamic structure than other aerial vehicles. As a result, developing a dependable flight control system for a DFAV is a difficult challenge, particularly during vertical flight [25-27]. The Environmental Control System (ECS) used in commercial aircraft is critical for dealing with the physiological and comfort requirements of passengers and crew. Heating, Ventilation, and Air Conditioning (HVAC) ductwork is regularly subjected to temperature changes and cyclic pressurization during operation. Karthigairajan et al. carried out a comparative study on conjugate heat transfer analysis in welded joints connected to a bypass valve and a trim air valve. The study suggested that the spherically connected circular duct design with D/d=3.84 and L/d=6 is the most effective and cost-efficient alternative for air conditioning duct design under major thermo-cyclic stress [28]. Ritschl et al. have experimentally proved the feasibility of using a ducted fan in the design of a micro- or ultralight aircraft. Preliminary experimental results demonstrate that the internal loss of flow energy is

less than 3%, making the usage of a "cold jet" propulsion unit feasible [29]. Daniel et al. proposed a method for simulating ducted fan drive systems for hybrid-electric small aircraft using mean line flow analysis techniques [30]. Alexiou et al. developed a design that consisted of two parts: the heat exchanger (HEX) fitted on the fixed-wing, tactical Blended-Wing-Body (BWB) Unmanned Aerial Vehicle (UAV) prototype, and the size of the cold air intake ducts. An analytical design approach was described for this design, and laboratory testing was carried out to validate the expected HEX prototype [31].

Enhancing the internal Computational Fluid Dynamics (CFD) toolset is crucial to meet the evolving needs and expectations of the general aviation industry. Our current focus is on propeller-driven small- and mid-sized aircraft, aiming to develop methods that can accurately account for the propeller-induced flow field using the virtual blade model described by Zipszer et al. [32]. Żółtak and Stalewski created and evaluated a preliminary design idea for integrating the TP100 turboprop engine into the I-23 aircraft. The design process began with a parametric, interactive approach. They presented preliminary design and optimization results for the air-intake system and engine nacelle. The work included fitting a turboprop engine into a tiny aircraft in a tractor configuration [33]. Zipszer et al. developed a CFD model to assess the flow field within the engine compartment and investigate the effect of propeller-induced flows. Then, flight test data for a prototype was gathered and compared to the analytical results. The CFD model employed the built-in 3D corrected Virtual Blade Model to calculate the flow field produced by the propeller, which incorporated the aircraft's whole external geometry [34].

The liquid/air heat exchanger, sometimes known as the radiator, is the main component of a liquid cooling system. The installation aims to provide sufficient cooling air to the radiator and exhaust warm air to the outside. Only 20% to 30% of the radiator's frontal surface may be the inlet area due to the velocity differential between the air velocity needed for the radiator and the external free flow [35]. Figure 2.1 shows a simplified system [36].

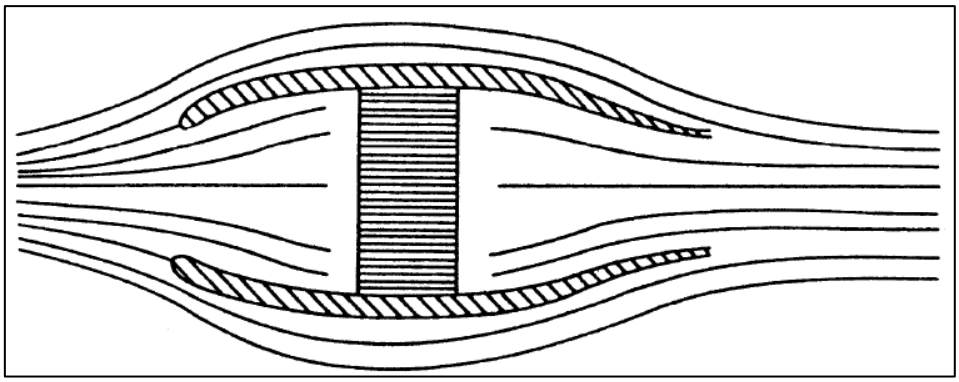

Figure 2.1: A simple ducted radiator design [36].

A basic installation for liquid cooling is shown in **Figure 2.2** [36]. Three distinct radiators, each with varying flow characteristics and requirements, are supplied through a shared inlet in this instance. Slanting radiators and/or allowing air to enter and depart at oblique angles relative to the radiator core ducts are frequently necessary due to existing interior volume limitations.

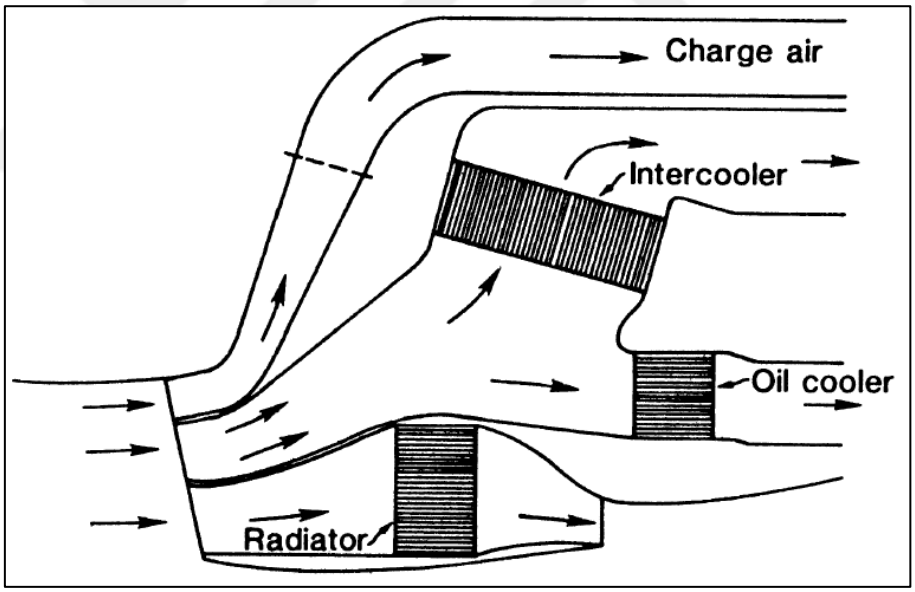

Figure 2.2: A simple ducted radiator design [36].

A large amount of research has been carried out on duct design and optimization. Using the example of an engine intake duct and coolant flow CFD, Okumura investigated the impact of tetrahedral and prismatic cell size and thickness on pressure loss and heat transfer coefficient. He discovered that the y+ distribution and pressure drop accuracy at the intake duct have improved due to the prismatic cell thickness and layer number on the wall. Additionally, the coolant flow simulation accuracy's heat

transfer coefficient has been enhanced [37]. Furlan et al. performed a multi-objective computational aerodynamic design optimization of an S-duct shape in their study, demonstrating that modifications to the wall curvature can minimize the ducts pressure loss and flow distortion in such a duct [38]. Mohler used the Wind-US flow solver to investigate the van effective and ineffective flow simulations on the M2129 diffuser type S-duct in his study. The simulations were performed using CFD software, and the outcomes were compared to the experimental data for distortion, total pressure recovery, and both with and without flow control. The computations and the experimental data were found to be in good agreement [39]. Prasath et al. performed CFD analyses for an aerodynamic body consisting of an S-entrance duct, a shallow ramp with curved walls recessed into the open surface, using Inviscid and Turbulent models (S-A, k-2, k-2). The research done for the various turbulence models shows that the global performance parameters match up well [40].

3. METODS AND MATERIALS

Aircraft is powered by piston engine which have twin turbo configuration. Thus two intercooler employed to manage the thermal property of charge air. Limit of pressure drop along turbocharger compressor outlet to intake manifold inlet and maximum inlet temperature at intake manifold value are determined by engine manufacturer. Hence declared pressure drop must not be exceeded during intercooler and piping design. Limit of pressure drop value ensures the engine run smoothly at idle setting. Temperature limit at entrance of manifold determines the climbing performance of aircraft at maximum power of engine. If outer pressure drop limit of designed heat exchanger is not met during climb, engine cooling will fail. In order to ensure the proper pressure drop from air flowing through heat exchangers whether climbing rate is decrease or throttle down the engine. Rule of thumb is to design the cooling system at the point where aircraft serve most of its time during whole operation envelope aka it is the cruise condition. Thus, smaller size heat exchanger fulfils the heat rejection rate without weight increase which is cause penalty. Smaller cooling component needs less air flowrate leading the smaller inlet duct that improve the aerodynamic and cooling drag properties. Hence cooling drag could be minimized without compromise performance. However, this rule causes some major performance problem at some regions such as temperature difference is considerably high between seasons. At hot seasons during climb at full power settings when aircraft at max take-off weight, engine confronts the situation like power loss due to high manifold temperature if cooling system is designed to cruise phase accordingly. Charge air and coolant liquid temperature elevation is inevitable during climb. High charge air temperature cause reduction at engine power. High coolant temperature cause raising of inner pressure at coolant circuit. Eventually pressure rise conclude coolant loss from expansion tank. It negatively effects climbing performance of aircraft and cause engine failure. On the other side oil temperature rise simultaneously with coolant and oil gets thinner hence it does not effectively lube the moving parts. If continuous climbing is dictated by requirements, design point must be the take-off phase of flight.

In this thesis two intercooler duct and one radiator duct will be designed. Two sets of duct group each contain three different inlet ducts designed by Unigraphics NX. Due to space restriction inside of nacelle, each heat exchanger place as effective as possible.

Twin turbo configuration needs two different size of intercooler hence each intercooler duct distinctive as their own. Inlet duct of radiator has simple shape relatively.

Intercoolers does not have exit ducts due to the tight packing of fuselage. There is risk of backflow through radiator exit duct if outgoing flow successfully blend into flow which is streaming over nacelle. Therefore, outlet duct should interfere with skin and stretch toward incoming flow. It is not yet elongate so much. Excessive elongation cause increase at drag value.

All ducts are design according to worst case scenario that aircraft would be face. Hot summer day and full throttle power setting at very beginning of climb stage is design point of duct. As a statement of metric ISA+28 at sea level temperature and ISA sea level altitude is accepted as design condition. Climbing rate and depending climb speed is determined by aircraft weight that accepted at maximum take-off weight. Hence 80 knots climb speed stand at intersection point of two requirements.

Location of duct entrance is just behind the propeller. Propeller create ram effect and this has positive impact on aerodynamic performance of duct.

Air mass flow rate which must be passing through heat exchanger is determined by manufacturer in order to obtain desired heat rejection at selected environmental condition. Air mass flow rate values and pressure drop limits is shown below table.

3.1. Requirement Definition

Aircraft powered by 100 kW twin turbocharger reciprocating engine. If there is no heat rejection data available, one third of the total power could be estimate as a heat dissipation rate. However generally engine manufacturer supplies required heat rejection rate. In this case component of cooling systems requirements are shown below tables.

Table 3.1: Radiator requirements.

Nomenclature	**Value**
External Fluid Inlet Temperature	43°C
Internal Fluid Inlet Temperature	85°C - 100°C
Inlet Fluid Flow	152 l/min
Internal Flow Pressure Difference	Max. 56 kPa
Internal Fluid Inlet Pressure (abs.)	1.52 – 1.68 bar
External Fluid Inlet Pressure (abs.)	1 bar
Cooling Capacity	52 kW

Table 3.2: Intercooler-1 requirements.

Nomenclature	**Value**
External Fluid Inlet Temperature	43°C
Internal Fluid Inlet Temperature	72°C
Internal Fluid Flow (Full Throttle)	528 kg/h
Internal Fluid Inlet Pressure (abs.)	1.6 bar
External Fluid Inlet Pressure	1 bar
Max. Turbocharger-2 Inlet Temperature	48°C

Table 3.3: Intercooler-2 requirements.

Nomenclature	**Value**
External Fluid Inlet Temperature	43°C
Internal Fluid Inlet Temperature	120°C
Internal Fluid Flow (Full Throttle)	528 kg/h
Internal Fluid Inlet Pressure (abs.)	2.4 bar
External Fluid Inlet Pressure	1 bar
Max. Manifold Air Temperature	48°C

Cooling systems are often designed based on the flight phase that occupies the majority of the aircraft's flight envelope. The cruising phase is when an aircraft spends the majority of its time in the flying envelope. The system designed according to this phase brings minimal aerodynamic drag and eliminates the need for excessively large cooling equipment. However, in places with a large temperature variation between seasons and day/night, a cooling system designed for a cruise cannot manage the heat created by the engine during take-off and climb in hot weather. If the climb continues without reducing the throttle with the system set to the cruising point, the cooling water temperature rises. The heat that cannot be dissipated raises the coolant temperature. Coolant that exceeds the safe limit temperature expands, increasing the system's internal pressure, and begins to be discharged through the expansion vessel when the amount of coolant circulating in the system falls below the minimum amount required by the engine for proper cooling, the cooling system can no longer reject the required heat. Due to overheating, the cylinder head gasket burns and causes the coolant to mix into the oil channels and combustion chamber. The coolant mixed into the oil system deteriorates the lubricating properties of the oil as a result wear increase. Continuous heating causes the engine to fail with the abrasions and cracks in the system. In aircraft where, continuous climbing is desired until the aircraft reaches the cruising altitude, the cooling system is designed according to the first minutes of the climb when the

thermal load is the highest. Thus, the overheating problem is prevented during the climb.

Table 3.4: Radiator specification.

Nomenclature	**Value**
Internal Fluid Flow (Full Throttle)	112 l/min
Internal Fluid Inlet Temperature	100°C
Internal Fluid Exit Temperature	91.5°C
Internal Fluid Inlet Pressure (abs.)	147.6 kPa
Internal Flow Pressure Difference	70.8 kPa
External Fluid Flow	1.76 kg/s
External Fluid Inlet Temperature	43°C
External Fluid Exit Temperature	60°C
External Fluid Inlet Pressure (abs.)	101.3 kPa
External Flow Pressure Difference	643.2 kPa
Cooling Capacity	59 kW

The aircraft, which is the subject of this paper, is required to climb continuously up to the cruise altitude at ISA+28 degrees ambient temperature with maximum weight. Therefore, the cooling system will be designed according to the requirement to increase aerodynamic and cooling friction compared to the cruise design point. Aircrafts forward speed is 80 knots during climb with maximum take-off weight.

Component manufacturer (intercooler and radiator) tests first prototype components and declares required amount of external airflow rate to achieve specified heat rejection rates. **Table 3.4**-**Table 3.6** show test result of components.

Table 3.5: Intercooler 1 specification.

Nomenclature	**Value**
Internal Fluid Flow	528 kg/h
Internal Fluid Inlet Temperature	88°C
Internal Fluid Exit Temperature	47°C
Internal Fluid Inlet Pressure (abs.)	1.6 bar
Internal Flow Pressure Difference	128.8 mbar
External Fluid Flow	0.57 kg/s
External Fluid Inlet Temperature	43°C
External Fluid Exit Temperature	46°C
External Fluid Inlet Pressure (abs.)	101.3 kPa
External Flow Pressure Difference	725.6 Pa
Cooling Capacity	7.68 kW

Table 3.6: Intercooler 2 specification.

Nomenclature	**Value**
Internal Fluid Flow	528 kg/h
Internal Fluid Inlet Temperature	132°C
Internal Fluid Exit Temperature	50°C
Internal Fluid Inlet Pressure (abs.)	2.4 bar
Internal Flow Pressure Difference	88.38 mbar
External Fluid Flow	0.58 kg/s
External Fluid Inlet Temperature	43°C
External Fluid Exit Temperature	55°C
External Fluid Inlet Pressure (abs.)	101.3 kPa
External Flow Pressure Difference	723.2 Pa
Cooling Capacity	15.8 kW

Air ducts must supply declared mass flow rate shown above.

3.2. Preliminary Design

Required inlet area of duct calculates preliminary based on mass continuity equation for incompressible flow that shown below:

$$Q = \rho \times A \times V \tag{3.1}$$

Perfect gas equation:

$$p = \rho \times R \times T \tag{3.2}$$

Mass flow rate dictated by component requirement, air density according to ISA+15 could be find:

$$\rho = \frac{p}{R \times T} \tag{3.3}$$

Hence preliminary inlet area of ducts could determine from (3.4) equation below

$$A = \frac{Q}{\rho \times V} \tag{3.4}$$

Appropriate velocity for the air through the duct is another parameter during preliminary design phase. This velocity should be high enough to ensure effective cooling but not so high to cause turbulence or excessive pressure losses. A typical range for cooling applications is 15-25 m/s, but this might vary depending on the aircraft and operational requirements. The cross section of the duct could be changed to achieve the required air velocity inside the duct.

Duct routes should be as short and direct as possible. Minimizing the length of ducts reduces the potential for pressure drops and energy loss, while fewer bends help maintain consistent airflow and reduce turbulence. It's advantageous to have at least a few diameters which is found in conversion of inlet area to equivalent area of circle length of straight ducting before the air enters the cooling component to ensure uniform flow distribution. The radius of any bend in the ductwork should be at least

three times the diameter of the duct. This rule helps to minimize pressure drops and flow separation that can occur in tighter bends. The smoother the transition in direction, the more efficient the airflow will be.

A 3D model of the air ducts was modelled using Siemens Unigraphics NX CAD software. **Figure 3.1** below shows an overview of configuration 1.

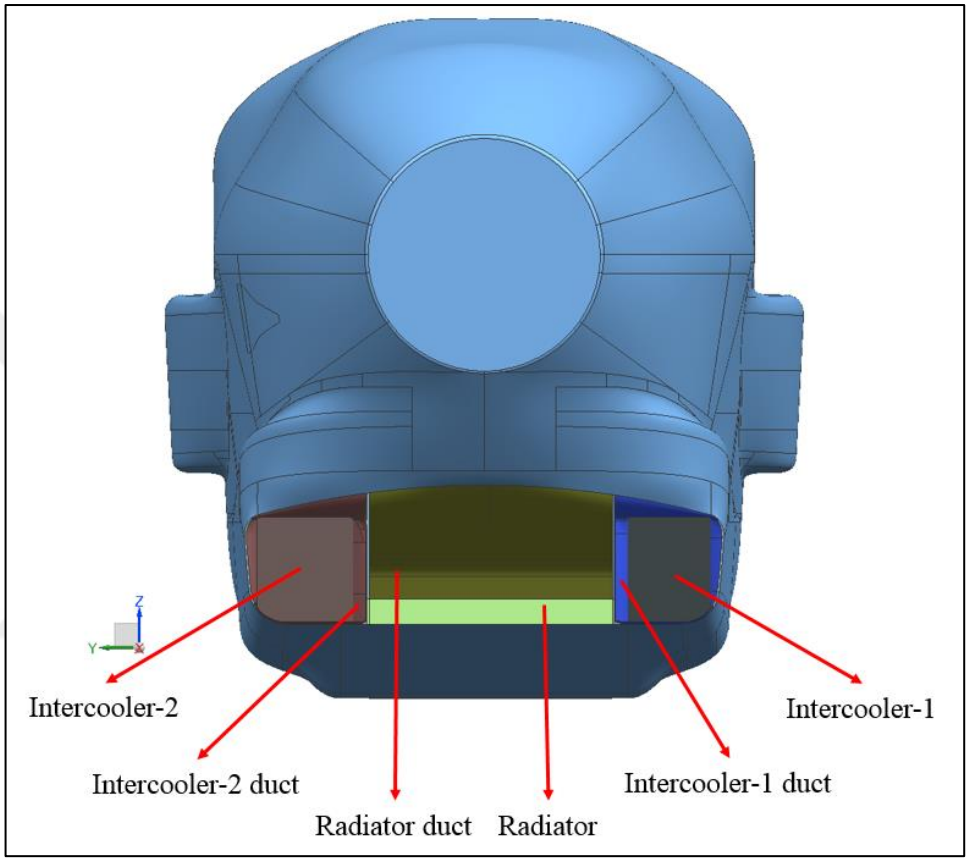

Figure 3.1: Overview of configuration 1.

Figure 3.2- Figure 3.3 shows details of intercooler-1 core and related inlet duct.

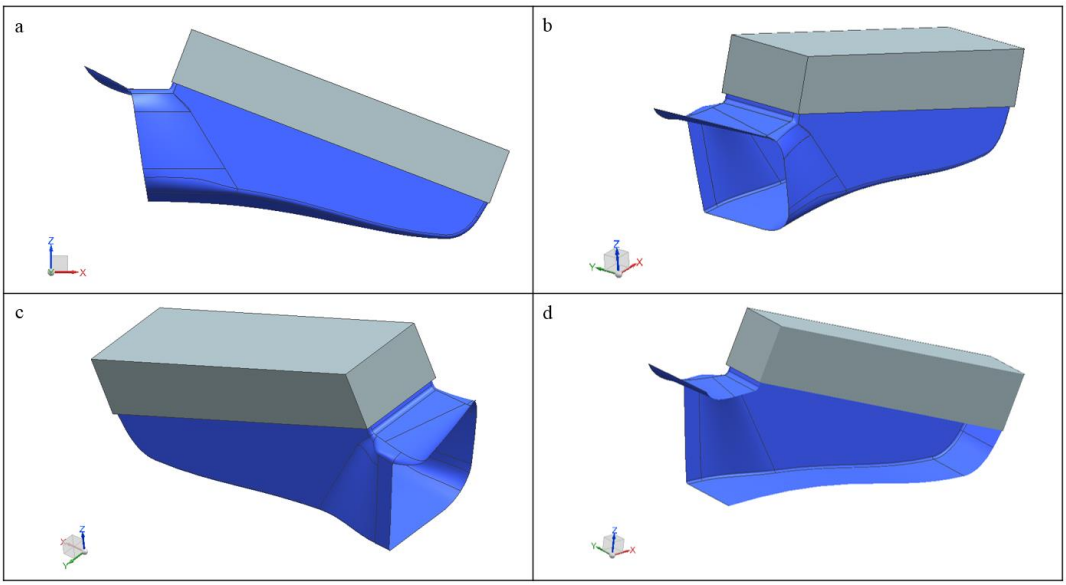

Figure 3.2: Detailed view of intercooler1-duct pair at configuration 1 a) left view, b) trimetric view from left, c) trimetric view from right, d) cross section view.

The inlet area of the intercooler-1 duct is 19973.128 mm^2 and the diameter of the circle with an area equivalent to the inlet area is 159.51 mm. The distance in the X direction between the centre of the inlet and exit area of the duct is 216.856 mm.

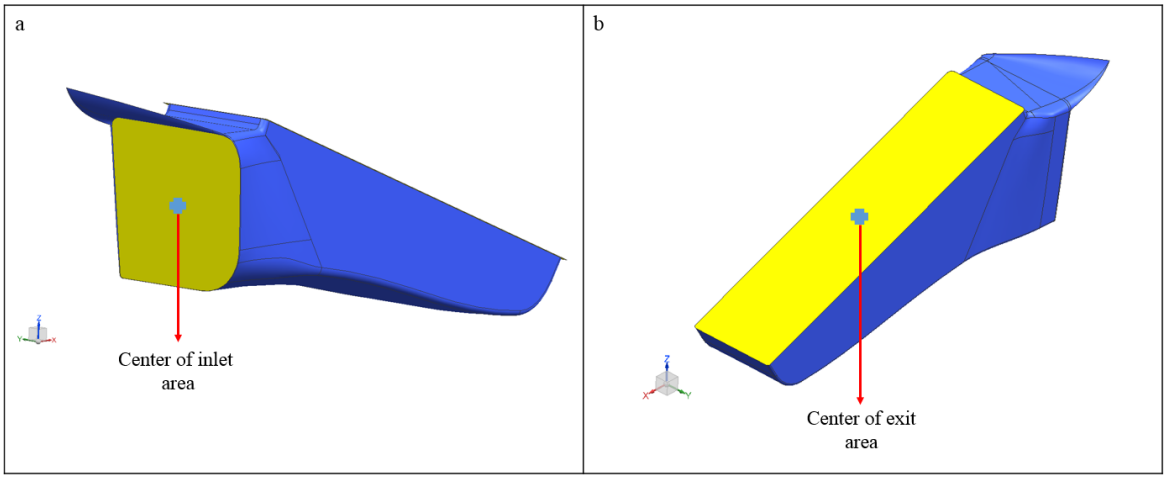

Figure 3.3: Centre of areas a) inlet, b) exit.

Figure 3.4- Figure 3.5 belong to intercooler-2 core and related inlet duct.

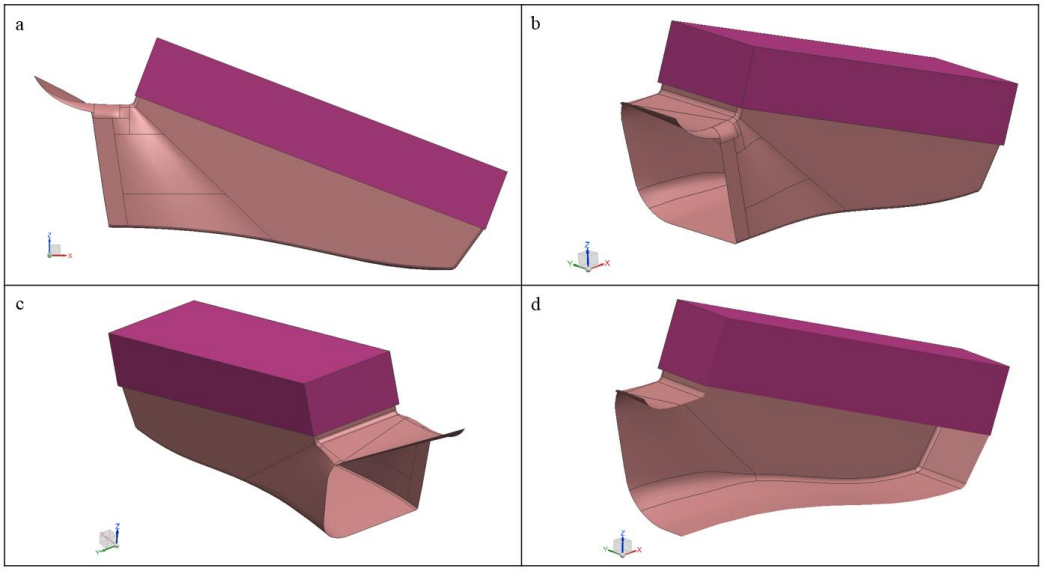

Figure 3.4: Detailed view of intercooler2-duct pair at configuration 1 a) left view, b) trimetric view from left, c) trimetric view from right, d) cross section view.

The inlet area of the intercooler-2 duct is 22370.736 mm^2 and the diameter of the circle with an area equivalent to the inlet area is 168.813 mm. The distance in the X direction between the centre of the inlet and exit area of the duct is 216.648 mm.

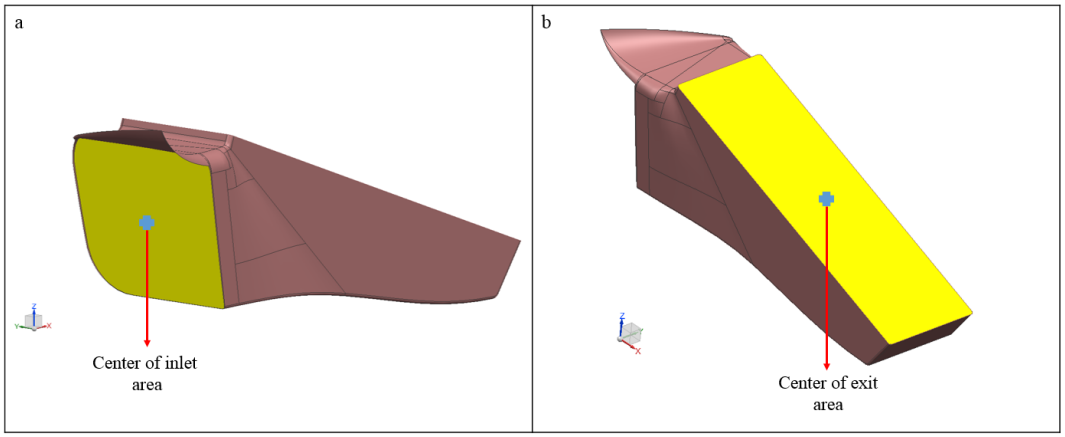

Figure 3.5: Centre of areas a) inlet, b) exit.

Figure 3.6- Figure 3.8 show radiator core and duct couple, which are the last ducts of configuration 1, are given on the following pages.

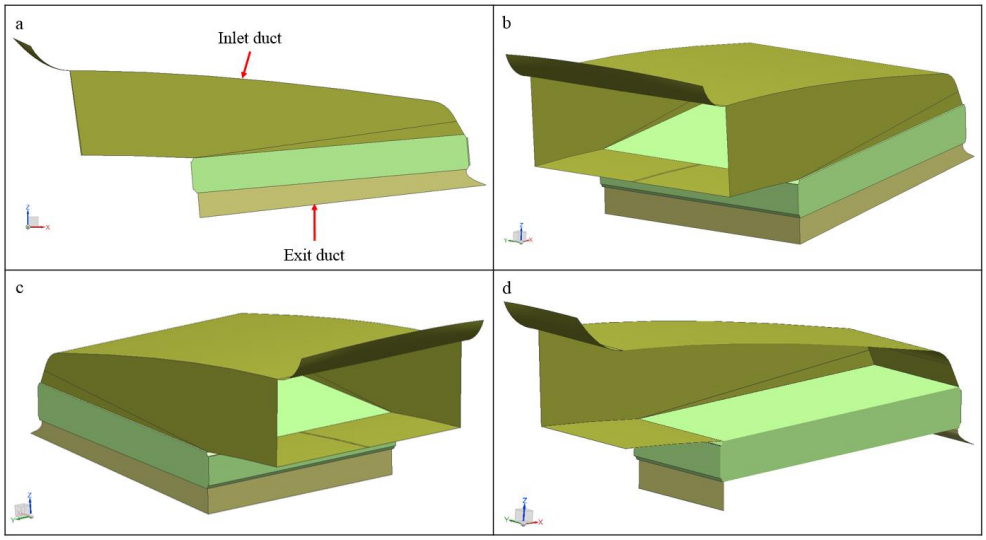

Figure 3.6: Detailed view of radiator core and duct couple at configuration 1 a) left view, b) trimetric view from left, c) trimetric view from right, d) cross section view.

The inlet area of the radiator inlet duct is 45192.681 mm^2 and the diameter of the circle with an area equivalent to the inlet area is 239.938 mm. The distance in the X direction between the centre of the inlet and exit area of the duct is 363.929 mm.

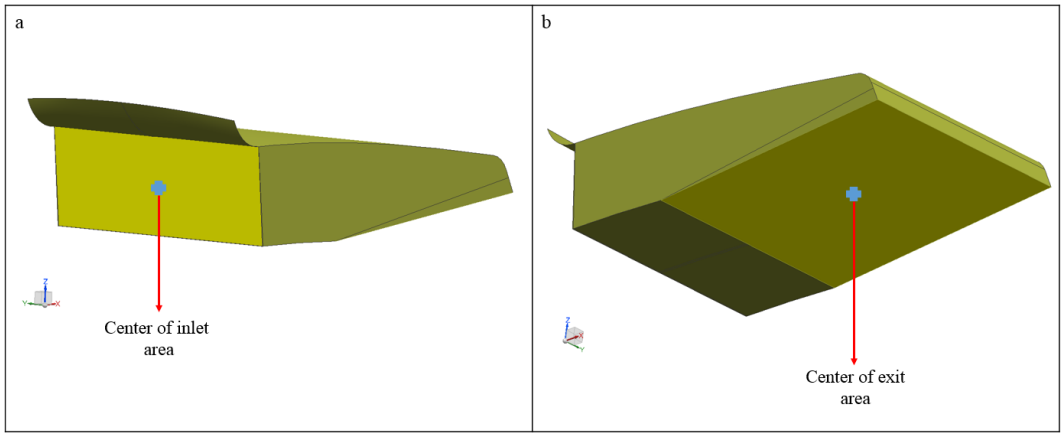

Figure 3.7: Centre of areas a) inlet, b) exit.

The inlet area of the radiator exit duct is 142635.165 mm^2 and the diameter of the circle with an area equivalent to the inlet area is 426,264 mm. The distance in the Z direction between the centre of the inlet and exit area of the exit duct is 29.023 mm.

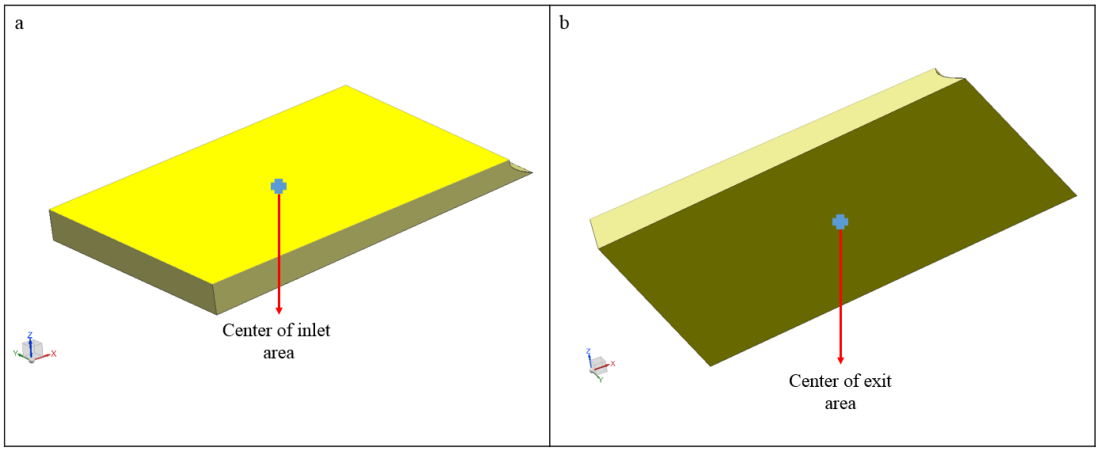

Figure 3.8: Centre of areas a) inlet, b) exit.

The following images which contain the radiator and both intercooler ducts belong to configuration 2. **Figure 3.9** shows an overview of configuration 1.

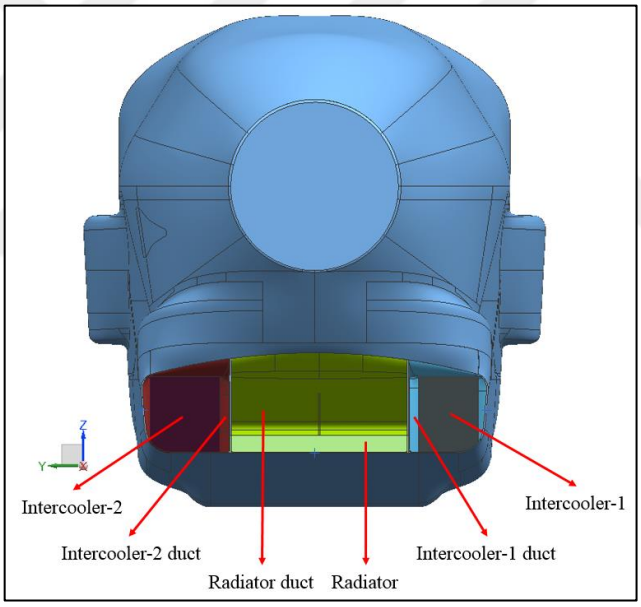

Figure 3.9: Overview of configuration 2.

Figure 3.10- Figure 3.11show details of duct and component couple of configuration 2. The figure below shows details of the intercooler-1 core and related inlet duct.

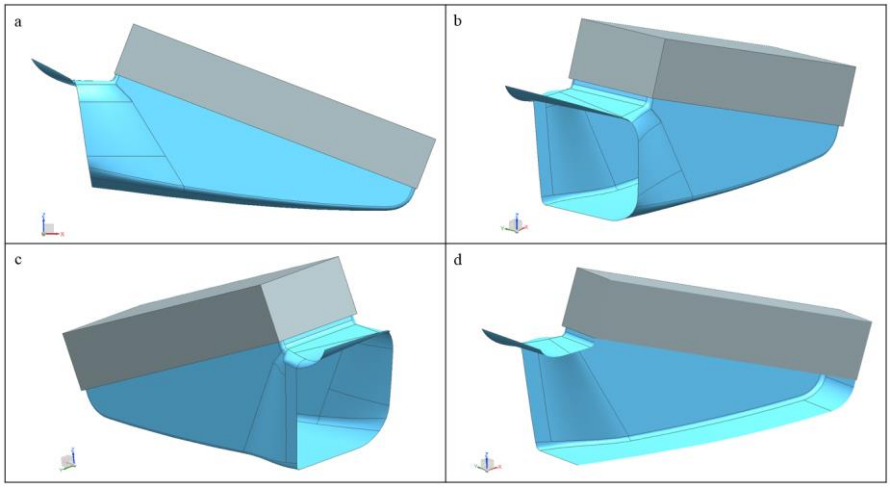

Figure 3.10: Detailed view of intercooler1-duct pair at configuration 2 a) left view, b) trimetric view from left, c) trimetric view from right, d) cross section view.

The inlet area of the intercooler-1 duct is 17480.429 mm^2 and the diameter of the circle with an area equivalent to the inlet area is 149.225 mm. The distance in the X direction between the centre of the inlet and exit area of the duct is 188.859 mm.

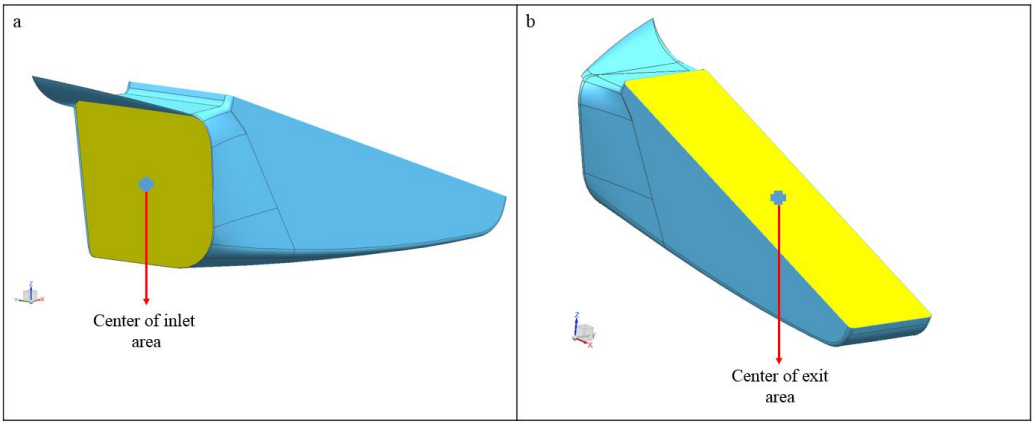

Figure 3.11: Centre of areas a) inlet, b) exit.

Figure 3.12- Figure 3.13belong to intercooler-2 core and related inlet duct.

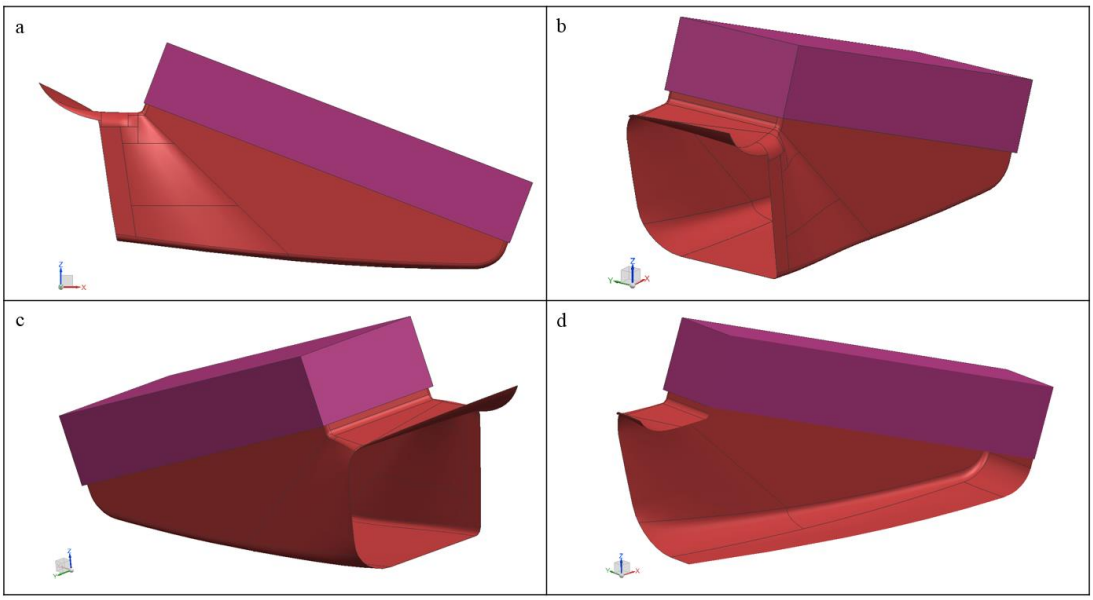

Figure 3.12: Detailed view of intercooler2-duct pair at configuration 2 a) left view, b) trimetric view from left, c) trimetric view from right, d) cross section view.

The inlet area of the intercooler-2 duct is 19591.905 mm^2 and the diameter of the circle with an area equivalent to the inlet area is 157.981 mm. The distance in the X direction between the centre of the inlet and exit area of the duct is 188.819 mm.

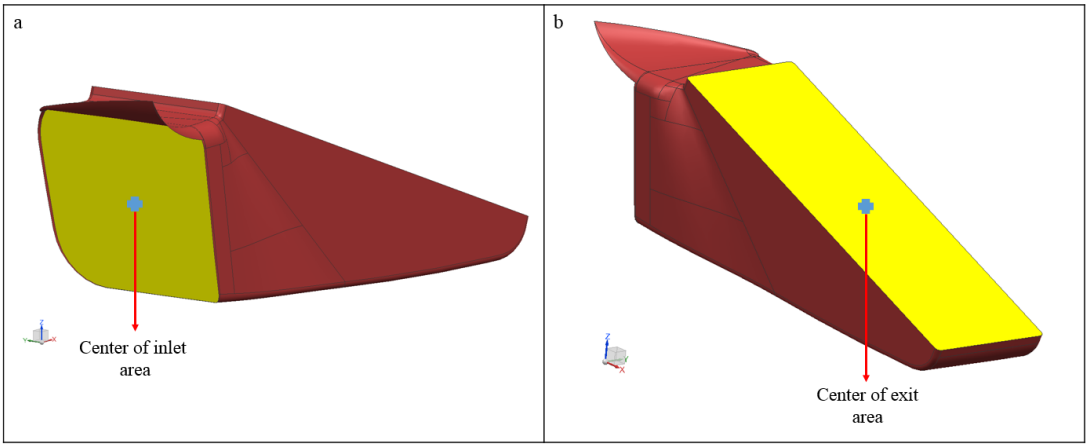

Figure 3.13: Centre of areas a) inlet, b) exit.

Figure 3.14-Figure 3.15 shows radiator core and inlet duct which are the last duct of configuration 2, are given on the following figures. Both configuration 1 and configuration 2 share same exit duct at outlet of radiator.

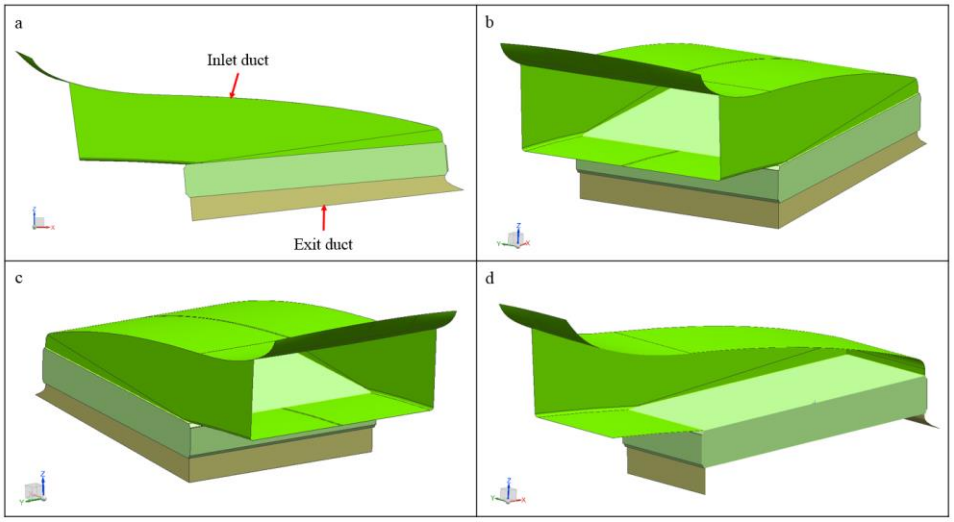

Figure 3.14: Detailed view of radiator core and duct couple at configuration 2 a) left view, b) trimetric view from left, c) trimetric view from right, d) cross section view.

The inlet area of the radiator inlet duct is 38255.029 mm^2 and the diameter of the circle with an area equivalent to the inlet area is 220.754 mm. The distance in the X direction between the centre of the inlet and exit area of the duct is 317.722 mm.

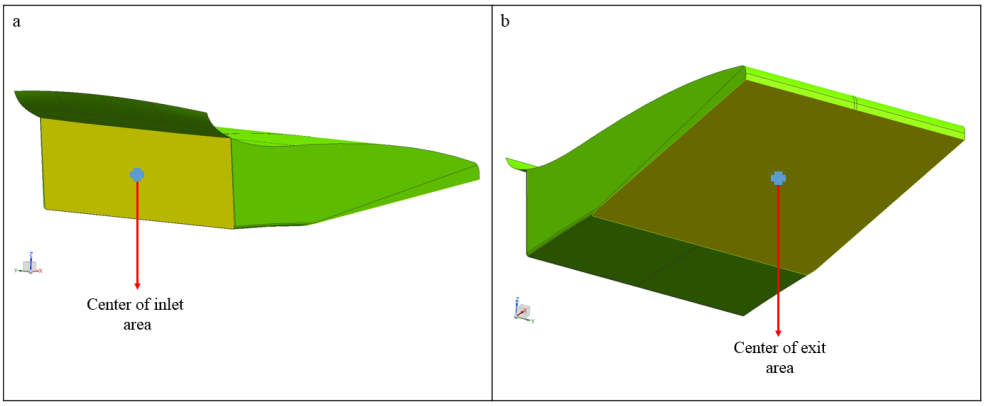

Figure 3.15: Centre of areas a) inlet, b) exit.

Figure 3.16 shows the difference in cross-sectional area between each duct option.

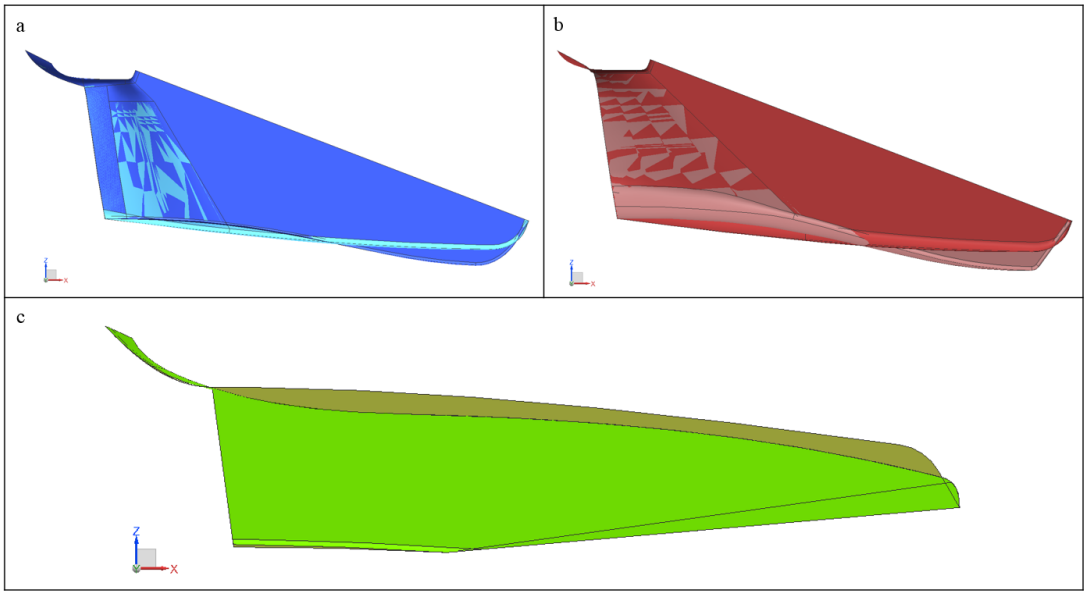

Figure 3.16: Cross sectional view of radiator, intercooler 1 and intercooler 2 ducts a) intercooler 1 ducts, b) intercooler 2 ducts, c) radiator ducts.

3.3. Analysis

Governing equation of fluid flow also help to construct mathematical basis for a comprehensive general-purpose model of fluid flow and heat transfer from the basic principles of conservation of mass, momentum and energy. The governing equations of fluid flow are mathematical formulations of mass conservation, momentum conservation and energy conservation. Below equations states the mass conservation in three dimensions [41].

$$\frac{\partial \rho}{\partial t} + \text{div}(\rho V) = 0 \tag{3.5}$$

In rectangular coordinates, the symbol V(x, y, z, t) denotes that the velocity of a fluid particle depends on where it is within the flow field and when it occupies the given location.

$$V = u\hat{\imath} + v\hat{\jmath} + w\hat{k} \tag{3.6}$$

u, v and w are the velocity components in the x, y, and z directions and be a function of x, y, z, t respectively. $\hat{\imath}$, $\hat{\jmath}$ and $\hat{k}$ are the corresponding unit vectors.

Assume that ϕ is the value of property per unit mass. Substantive derivative of ϕ with respect to time following a fluid particle,

$$\frac{D\phi}{Dt} = \frac{\partial\phi}{\partial t} + u\frac{\partial\phi}{\partial x} + v\frac{\partial\phi}{\partial y} + w\frac{\partial\phi}{\partial z} = \frac{\partial\phi}{\partial t} + V \cdot grad\phi \tag{3.7}$$

$D\phi/Dt$ defines rate of change of property ϕ per unit mass. If $D\phi/Dt$ multiply by density ρ, rate of change of property ϕ per unit volume obtain.

$$\rho\frac{D\phi}{Dt} = \rho\left(\frac{\partial\phi}{\partial t} + V \cdot grad\phi\right) \tag{3.8}$$

Generalize of mass conservation equation for an arbitrary conserved property ϕ to express the relation among the rate of increase of ϕ for a fluid particle, the rate of change in time of ϕ per unit volume and the net flow of ϕ out of the fluid element per unit volume:

$$\frac{\partial\rho\phi}{\partial t} + div(\rho\phi V) = \rho\frac{D\phi}{Dt} \tag{3.9}$$

From the generalized form of above equation, three components of momentum equation and the energy equation could be derived as shown below:

$$\rho\frac{Du}{Dt} = \frac{\partial(\rho u)}{\partial t} + div(\rho u V) \tag{3.10}$$

$$\rho\frac{Dv}{Dt} = \frac{\partial(\rho v)}{\partial t} + div(\rho v V) \tag{3.11}$$

$$\rho\frac{Dw}{Dt} = \frac{\partial(\rho w)}{\partial t} + div(\rho w V) \tag{3.12}$$

$$\rho \frac{DE}{Dt} = \frac{\partial(\rho E)}{\partial t} + div(\rho EV) \tag{3.13}$$

It is convenient to classify forces exerted on the fluid particle as body forces and surface forces in two categories. Pressure forces, viscous forces, and gravity forces are examined as surface forces as well as centrifugal forces, Coriolis forces, and electromagnetic forces scope under body forces.

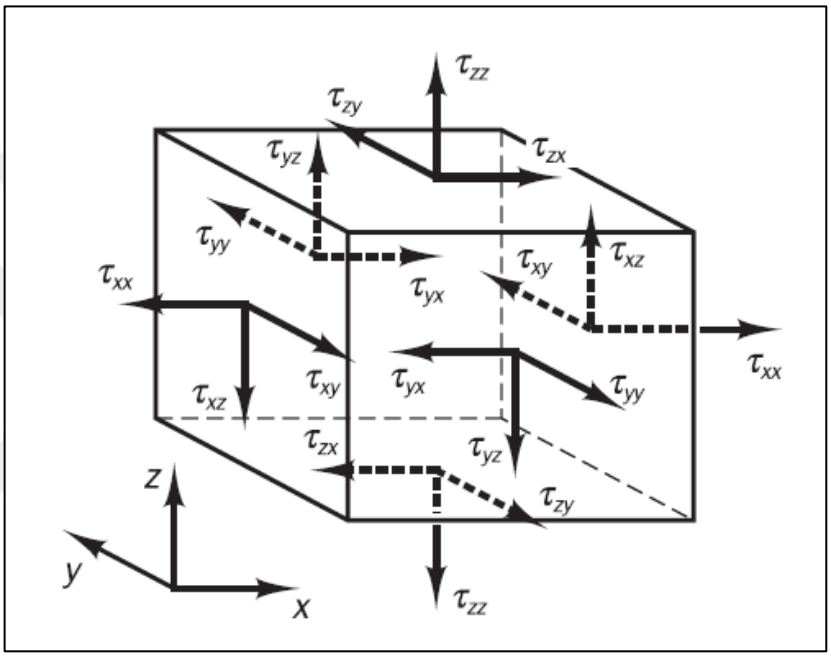

Figure 3.17: Stress components on three faces of fluid element [41].

It is widely accepted to stress the contributions of surface forces as separate components in the momentum equation, while including the effects of body forces as source terms. Body forces at x, y, z direction will be denoted by S_{Mx}, S_{My}, S_{Mz} subsequently as a source term.

The heat flux vector q is composed by q_x, q_y, q_z and local temperature gradient was connected to the heat flux by Fourier's law of heat conduction. Hence

$$q_x = -k\frac{\partial T}{\partial x} \quad q_y = -k\frac{\partial T}{\partial y} \quad q_z = -k\frac{\partial T}{\partial z} \tag{3.14}$$

Above gradients express in the vector form as:

$$q = -k\ grad\ T \tag{3.15}$$

Energy of a fluid is generally defined as the sum of internal (thermal) energy, kinetic Energy, and gravitational potential energy. In mathematical term

$$E = i + \frac{1}{2}(u^2 + v^2 + w^2) + S_e \tag{3.16}$$

i stands for internal/thermal energy, $\frac{1}{2}(u^2 + v^2 + w^2)$ for kinetic energy, S_E ,source term, potential energy changes per unit volume per unit time. Rate of increase of energy of a fluid particle per unit volume is also defined as sum of the net rate of work done on the fluid particle, the net rate of heat addition to the fluid and the rate of increase of energy due to sources.

$$\begin{aligned}\rho\frac{DE}{Dt} &= -div(pV) \\ &+ \left[\frac{\partial(u\tau_{xx})}{\partial x} + \frac{\partial(u\tau_{yx})}{\partial y} + \frac{\partial(u\tau_{zx})}{\partial z} + \frac{\partial(v\tau_{xy})}{\partial x}\right. \\ &+ \frac{\partial(v\tau_{yy})}{\partial y} + \frac{\partial(v\tau_{zy})}{\partial z} + \frac{\partial(w\tau_{xz})}{\partial x} + \frac{\partial(w\tau_{yz})}{\partial y} \\ &\left.+ \frac{\partial(w\tau_{zz})}{\partial z}\right] + div(k\ grad\ T) + S_E\end{aligned} \tag{3.17}$$

Conservation equation for the kinetic energy can be obtain by multiplying the x-momentum equation by velocity component u, y-momentum equation by velocity component v, z-momentum equation by velocity component w and to sum results together.

$$\begin{aligned}&\rho\frac{D\left[\frac{1}{2}(u^2 + v^2 + w^2)\right]}{Dt} \\ &= -V \cdot grad\ p + u\left(\frac{\partial\tau_{xx}}{\partial x} + \frac{\partial\tau_{yx}}{\partial y} + \frac{\partial\tau_{zx}}{\partial z}\right) \\ &+ v\left(\frac{\partial\tau_{xy}}{\partial x} + \frac{\partial\tau_{yy}}{\partial y} + \frac{\partial\tau_{zy}}{\partial z}\right) + w\left(\frac{\partial\tau_{xz}}{\partial x} + \frac{\partial\tau_{yz}}{\partial y} + \frac{\partial\tau_{zz}}{\partial z}\right) + V \cdot S_M\end{aligned} \tag{3.18}$$

In order to obtain internal energy equation (3.20) subtracting (3.18) from (3.17) and define new source term as

$$S_i = S_E - V \cdot S_M \tag{3.19}$$

$$\begin{aligned}\rho \frac{Di}{Dt} = -p div(V) + div(k\ grad\ T) + \tau_{xx}\frac{\partial u}{\partial x} + \tau_{yx}\frac{\partial u}{\partial y} + \tau_{zx}\frac{\partial u}{\partial z} \\ + \tau_{xy}\frac{\partial v}{\partial x} + \tau_{yy}\frac{\partial v}{\partial y} + \tau_{zy}\frac{\partial v}{\partial z} + \tau_{xz}\frac{\partial w}{\partial x} + \tau_{yz}\frac{\partial w}{\partial y} \\ + \tau_{zz}\frac{\partial w}{\partial z} + S_i\end{aligned} \tag{3.20}$$

CFD study for duct design and cooling component efficacy is essentially based on the Navier-Stokes equations, which describe the motion of viscous fluid substances. These equations, along with energy conservation equations, enable detailed simulations of airflow dynamics and heat transfer. Navier-Stokes equations can be written in the most useful form for the development of the finite volume method:

$$\rho \frac{Du}{Dt} = -\frac{\partial p}{\partial x} + div(\mu\ grad\ u) + S_{Mx} \tag{3.21}$$

$$\rho \frac{Dv}{Dt} = -\frac{\partial p}{\partial y} + div(\mu\ grad\ v) + S_{My} \tag{3.22}$$

$$\rho \frac{Dw}{Dt} = -\frac{\partial p}{\partial z} + div(\mu\ grad\ w) + S_{Mz} \tag{3.23}$$

Implementation of the Newtonian model for viscous stresses is used in the internal energy equation with a little bit of manipulation

$$\rho \frac{Di}{Dt} = -p\ div\ V + div(k\ grad\ T) + \Phi + S_i \tag{3.24}$$

can be obtained. Dissipation functionΦ, describes the all effects because of viscous stresses in thermal energy equation.

$$\Phi = \mu\left\{2\left[\left(\frac{\partial u}{\partial x}\right)^2+\left(\frac{\partial v}{\partial y}\right)^2+\left(\frac{\partial w}{\partial z}\right)^2\right]+\left(\frac{\partial u}{\partial y}+\frac{\partial v}{\partial x}\right)^2 + \left(\frac{\partial u}{\partial z}+\frac{\partial w}{\partial x}\right)^2+\left(\frac{\partial v}{\partial z}+\frac{\partial w}{\partial y}\right)^2\right\}+\lambda(div\ V)^2 \tag{3.25}$$

Perfect gas equation and specific internal energy states at below

$$p = \rho RT \tag{3.26}$$

$$i = C_v T \tag{3.27}$$

Equations that govern the time-dependent three-dimensional fluid flow and heat transfer of a compressible Newtonian fluid are reorganized below [41].

$$\frac{\partial \rho}{\partial t} + div(\rho V) = 0 \tag{3.28}$$

$$\frac{\partial(\rho u)}{\partial t} + div(\rho u V) = -\frac{\partial p}{\partial x} + div\ (\mu\ grad\ u) + S_{Mx} \tag{3.29}$$

$$\frac{\partial(\rho v)}{\partial t} + div(\rho v V) = -\frac{\partial p}{\partial y} + div\ (\mu\ grad\ v) + S_{My} \tag{3.30}$$

$$\frac{\partial(\rho w)}{\partial t} + div(\rho w V) = -\frac{\partial p}{\partial z} + div\ (\mu\ grad\ w) + S_{Mz} \tag{3.31}$$

$$\frac{\partial(\rho i)}{\partial t} + div(\rho i V) = -p\ div\ V + div(k\ grad\ T) + \Phi + S_i \tag{3.32}$$

Based on the above equations, computational fluid dynamics analysis were performed using Star CCM software by Siemens. The surface of the aircraft fuselage and the surface of the ducts are meshed with triangular mesh shown in **Figure 3.18**.

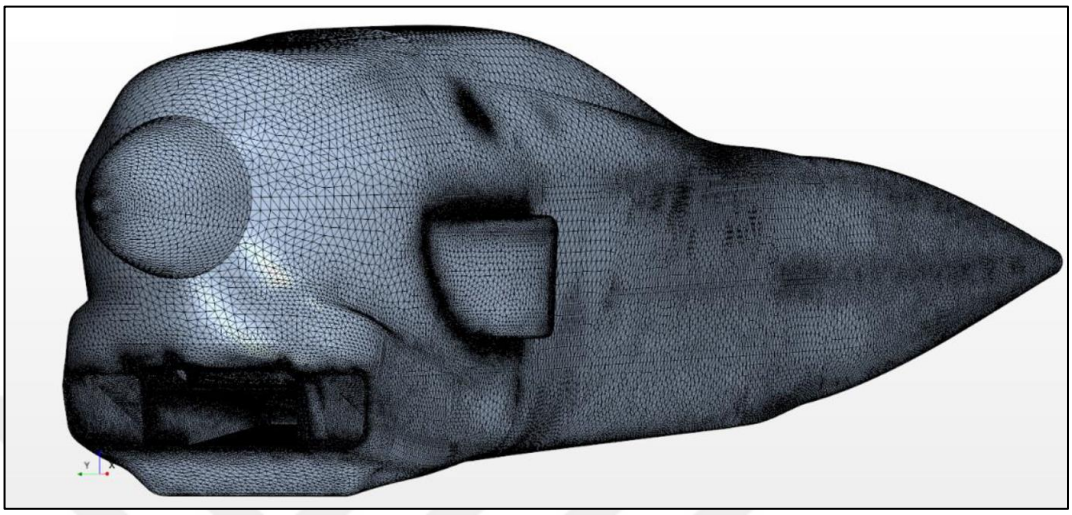

Figure 3.18: Surface mesh of aircraft fuselage.

Polygon mesh was employed to fill the volume of inspected space. It is seen at **Figure 3.19** and **Figure 3.20**.

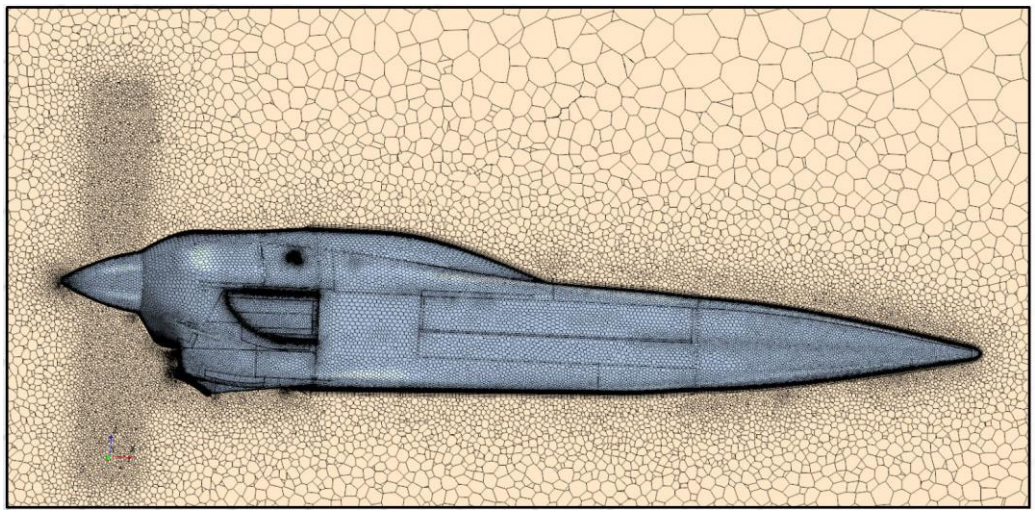

Figure 3.19: Volume mesh of inspected space.

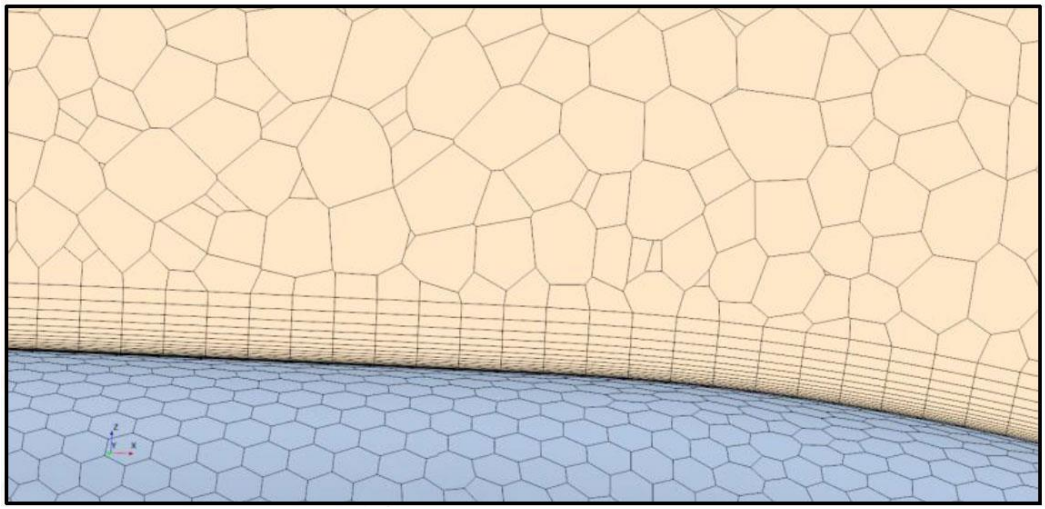

Figure 3.20: Detail view of volume mesh.

First wall spacing is the distance between the wall and the centre of the first cell (or layer) in the boundary layer mesh adjacent to the wall. To estimate wall shear stress, heat transfer, and boundary layer development, the velocity gradient and thermal gradient at the wall must be precisely captured. Hence first wall space distance estimated 5.10^{-6} m. y+ value is selected 1 in order to better capture boundary layer and wall effect. 5 million mesh cells created for analysis setup and mesh skewness value is 89º. k-w SST turbulence model is used in analysis due to its robustness in predicting separation and accurately capturing boundary layers. Ideal gas and constant velocity assumptions are made for the free stream boundary conditions. The analysis are conducted at sea level ISA +28 Cº (101325 pa, 43º). Engine thrust is determined at maximum performance and the speed of the aircraft at 80 knots. Blade Element Method is employed to include the propeller effect. The porous region has been defined by experimental data for the radiator and intercooler sections. NTU Epsilon approach is used to calculate heat transfer for radiator and intercooler parts. Wall boundary condition that is specify no-slip condition is defined for all solid surfaces.

4. RESULT AND DISCUSSION

The heat transfer rate for the radiator at configuration 1 is obtained from the analysis result shown in **Table 4.1:** Radiator thermal performance. The required heat rejected rate is demanded by the engine manufacturer 52 kW. Results show that the radiator-duct couple is designed according to fulfil requirements.

Table 4.1: Radiator thermal performance.

Radiator			
Δp (Pa)	Velocity (m/s)	Q (kg/s)	Heat Transfer(kW)
643.2	9.1	1.8	56.56

Exit temperature of intercooler 1 must not exceed 48 ºC. Intercooler 1-duct at configuration 1 cool down the inlet air to 45.6 ºC. Analysis result belongs to intercooler 1 can be seen at **Table 4.2**.

Table 4.2: Intercooler 1 thermal performance.

Intercooler 1				
Δp (Pa)	Velocity (m/s)	Q (kg/s)	Heat Transfer(kW)	T_{exit} (ºC)
1728	8.88	0.6	7.92	45.6

Intercooler 2 fulfil the demand of engine and provide air to manifold at temperature 47.52 ºC. Performance metric of intercooler 2 seen at **Table 4.3**.

Table 4.3: Intercooler 2 thermal performance.

Intercooler 2				
Δp (Pa)	Velocity (m/s)	Q (kg/s)	Heat Transfer(kW)	T_{exit} (°C)
1788	8.96	0.71	15.76	47.52

Velocity profile through the duct determines the mass flow rate that duct transfer efficiently end to end. Velocity profile at the inlet of the ducts is seen **Figure 4.1**. Reverse flow zones form at the upper part of the intercooler 2 and radiator duct. Reason of that behaviour is slipstream effect of propeller. The other possible cause is flow separation, which is similar to a loss of expansion loss. Fluid particles could not follow the shape of entrance lip easily due sharp turning radius of the entrance lip. This leads flow separation at upper region.

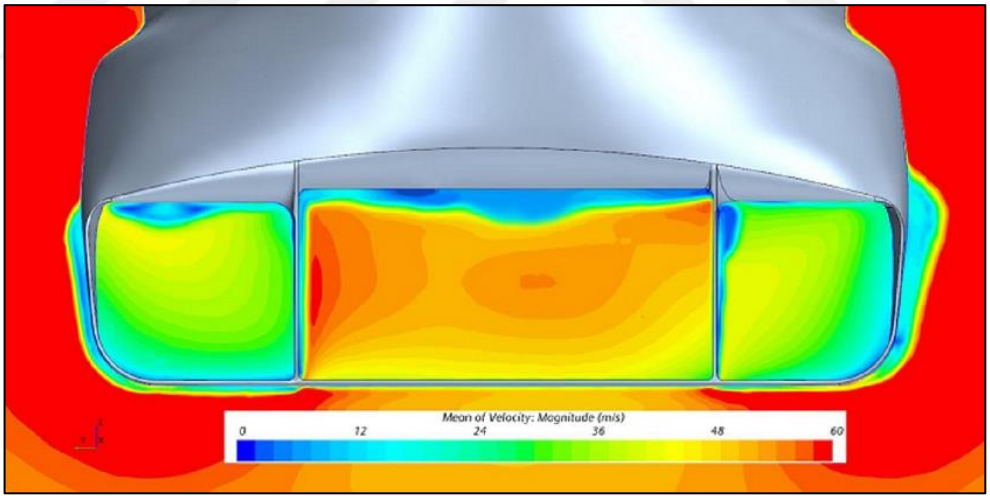

Figure 4.1: Velocity profile of ducts at inlet.

The cross-sectional view of the inlet region where the velocity profile drops to zero is shown in **Figure 4.2**. Combined effect of propeller slip stream, speed of the aircraft does not allow to air particle follow the lip contour. If turn radius of lip increase, flow separation area probably shrinks.

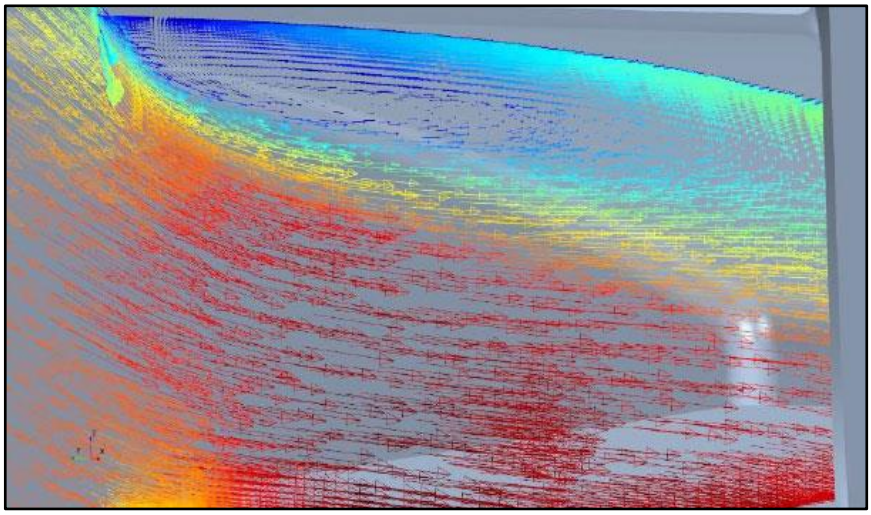

Figure 4.2: Cross sectional view of radiator duct at bisector plane.

Velocity profile of radiator exit can be seen at **Figure 4.3**. Airstream does not choke anywhere above radiator exit surface. However, velocity profile is not uniform hence this negatively affect performance of radiator. Airflow direct as perpendicular as possible with the help of duct at right side of radiator. There air pass directly and does not loss much energy. If velocity distribution occurs much even, cooling drags stays at lower level.

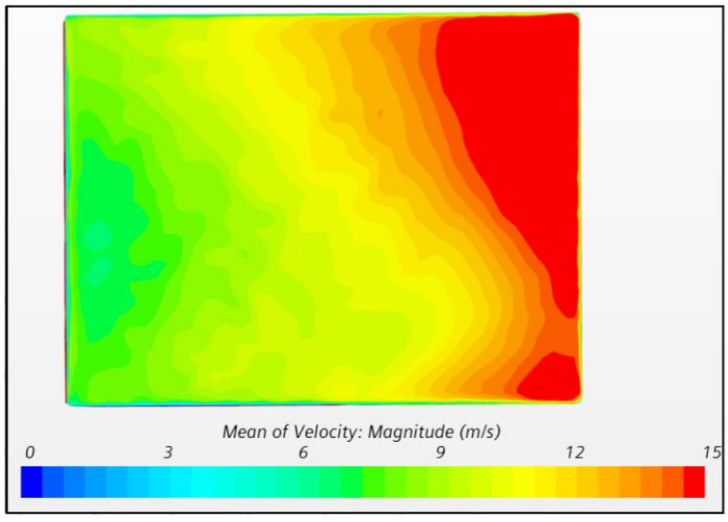

Figure 4.3: Velocity profile at the exit of radiator.

Velocity distribution belongs to intercoolers seen at **Figure 4.4** and **Figure 4.5**.

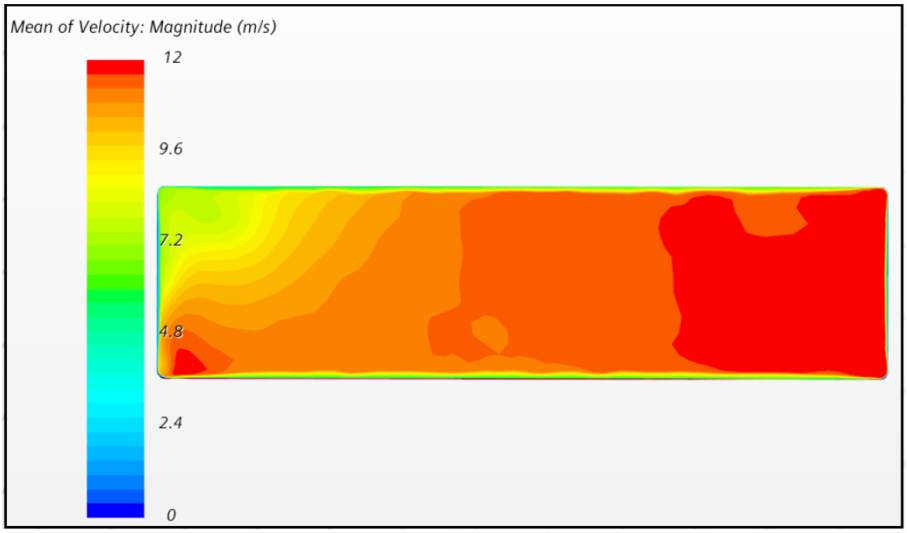

Figure 4.4: Velocity profile at the exit of intercooler 1.

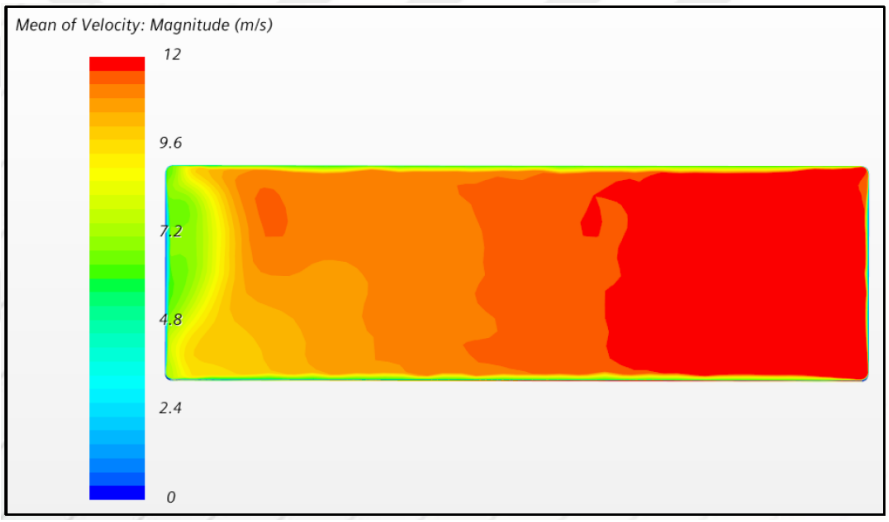

Figure 4.5: Velocity profile at the exit of intercooler 2.

Intercoolers placed more perpendicular with respect to radiator. This placement dramatically affects the velocity distribution over the exit. Left side of the intercoolers stay in the shadow of the duct due to its routing. It shows the affect as a low velocity area. Therefore, each intercooler individual contribution to the cooling drag much less than single radiator.

After verifying the performance of intercooler and radiator air ducts and cooling system components through analysis, the prototype production stage was initiated. The prototype air ducts used in this stage were manufactured using Ultem PEI AM9085F material with the assistance of 3D printers.

After the 3D printing process was completed, the air ducts were coated with three layers of prepreg material to increase their strength. During this coating process, the unidirectional fabric layers were laid up with 45/0/45 configuration, and then cured in an autoclave. This method allowed for savings in time, labour, and costs during rapid prototyping without the need for mold production.

Table 4.4: Mechanical properties of ULTEM AM9085F.

Property	Test Method	XY Orientation	XZ Orientation	ZX Orientation
Tensile Strength, Ultimate	ASTM D638	74 ± 4 MPa	80 ± 4 MPa	38 ± 3 MPa
Tensile Modulus	ASTM D638	2,490 MPa	2,590 MPa	2,430 MPa
Tensile Elongation at Break	ASTM D638	4.3%	7.1%	1.7%
Flexural Strength	ASTM D790	115 MPa	-	60 MPa
Flexural Modulus	ASTM D790	2,470 MPa	-	2,110 MPa
Flexural Strain at Break	ASTM D790	No Break	-	3%
Flexural Strain (Extension) at Tensile Strength	ASTM D790	7.3%	-	-
IZOD Impact, Notched	ASTM D256	134 J/m	-	-
IZOD Impact, Un-notched	ASTM D256	989 J/m	-	135 J/m
Compressive Strength, Yield	ASTM D695	100 MPa	-	103 MPa

Ultem PEI 9085 material is known for its high temperature resistance and mechanical strength properties, which played a significant role in enhancing the performance of the air ducts. Additionally, the use of 3D printers provided flexibility in the production process and enabled rapid adaptation to design changes.

In conclusion, prototype production using this method offered a faster and more economical solution compared to traditional mold production methods. It also provided significant advantages during the performance validation phase of the design.

After the assembly of the manufactured air ducts, intercooler, and radiator onto the aircraft, the performance of the cooling system will be evaluated. Ideally, testing the system in a wind tunnel before installation on the aircraft is a more rational approach. However, due to the lack of wind tunnels in every production facility, the study addressed in this thesis conducted its testing activities through flight tests.

Figure 4.6 displays the temperature of the air entering Turbo 1 from the outside environment. The turbo inlet temperature sensor, located at the filter inlet, measures both the ambient temperature and the incoming air temperature. Data obtained from this sensor is equivalent to the external fluid inlet temperature. The air entering Turbo 1 is directed to Intercooler 1 for compression and cooling. The air entering Intercooler 1 is shown in **Figure 4.7**. As engine power increases during the initial phase of takeoff, the temperature of the air entering Intercooler 1 reaches up to 89 degrees Celsius. Subsequently, the air exiting Intercooler 1 is cooled to 43 degrees Celsius as it exits the system (**Figure 4.8**). The exiting air is then directed to Turbocharger 2. The air exiting Turbocharger 2 is conveyed to Intercooler 2. As depicted in **Figure 4.9**, the temperature of the air entering Intercooler 2 reaches up to 108 degrees Celsius. The air exiting Intercooler 2 reaches the manifold inlet at 40 degrees Celsius, as shown in **Figure 4.10**, before entering the engine combustion chamber.

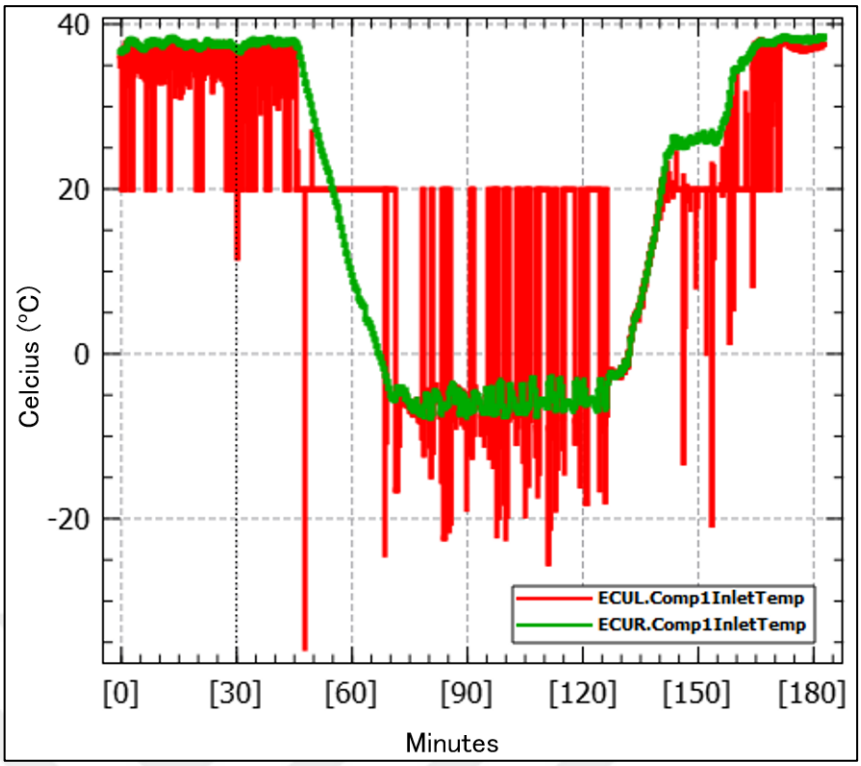

Figure 4.6: Turbocharger 1 inlet temperature versus time.

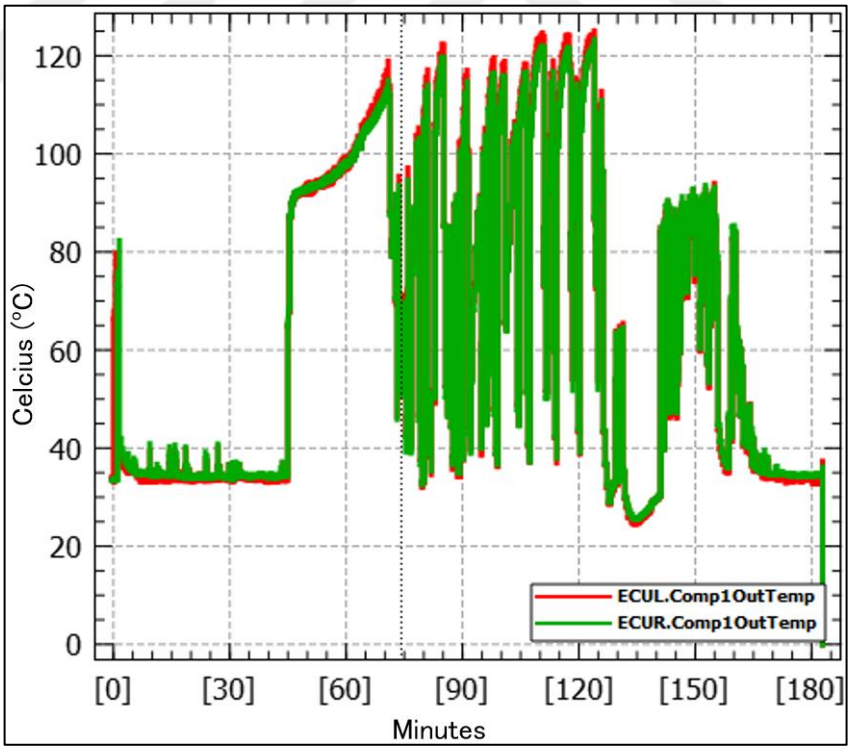

Figure 4.7: Turbocharger 1 outlet temperature versus time.

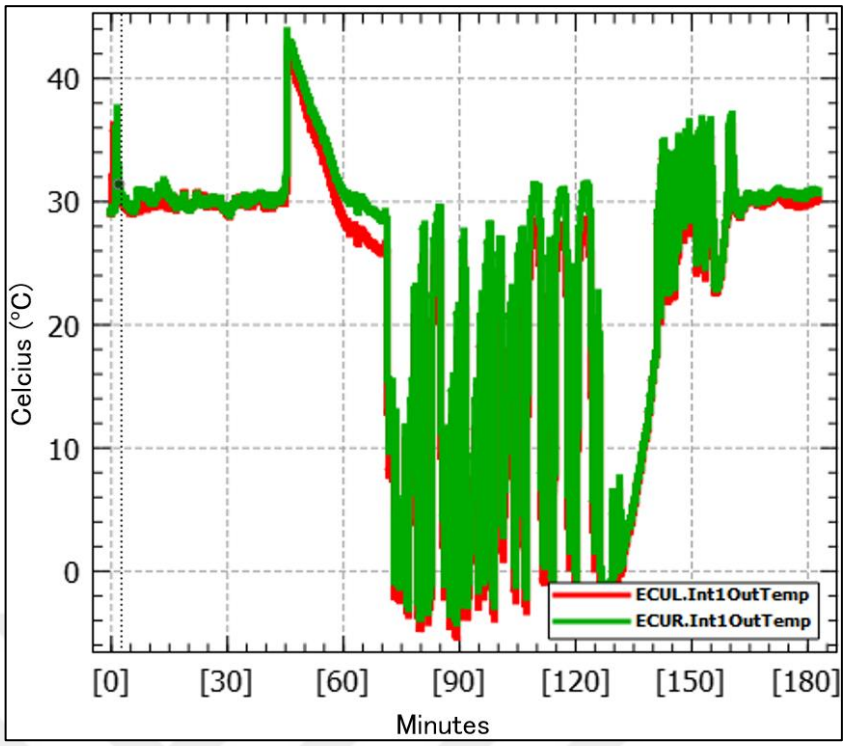

Figure 4.8: Intercooler 1 outlet temperature versus time.

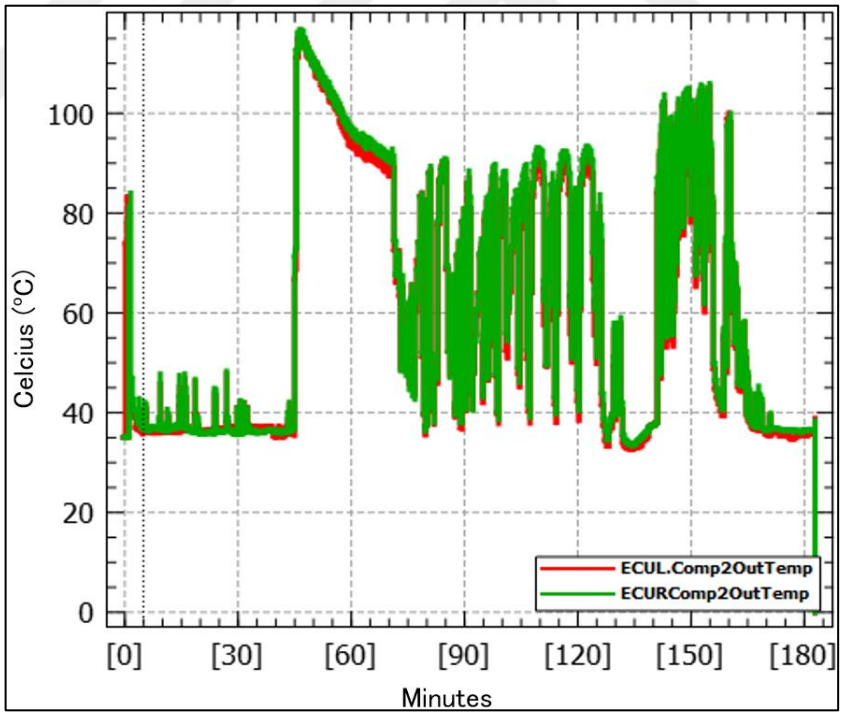

Figure 4.9: Turbocharger 2 outlet temperature versus time.

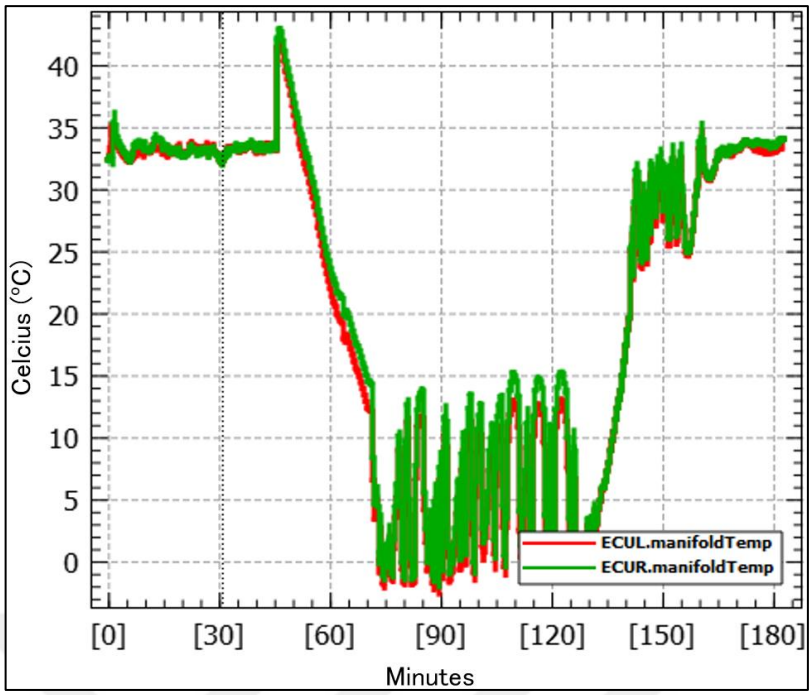

Figure 4.10: Manifold temperature versus time.

Figure 4.12a illustrates the barometric pressure recorded during flight tests. **Figure 4.12b** displays the engine power demand as indicated by the throttle position.

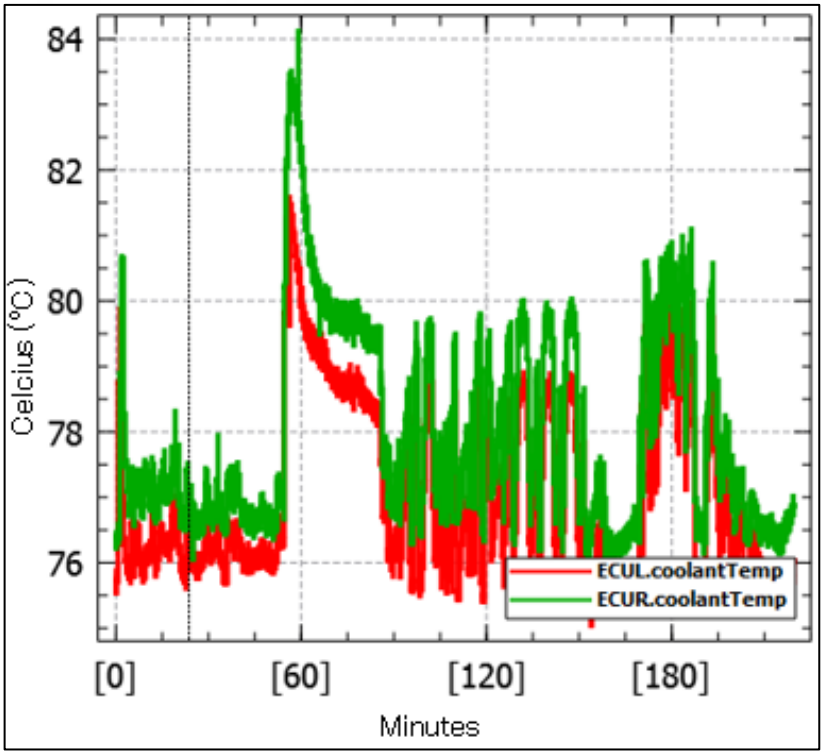

Figure 4.11: Coolant temperature versus time

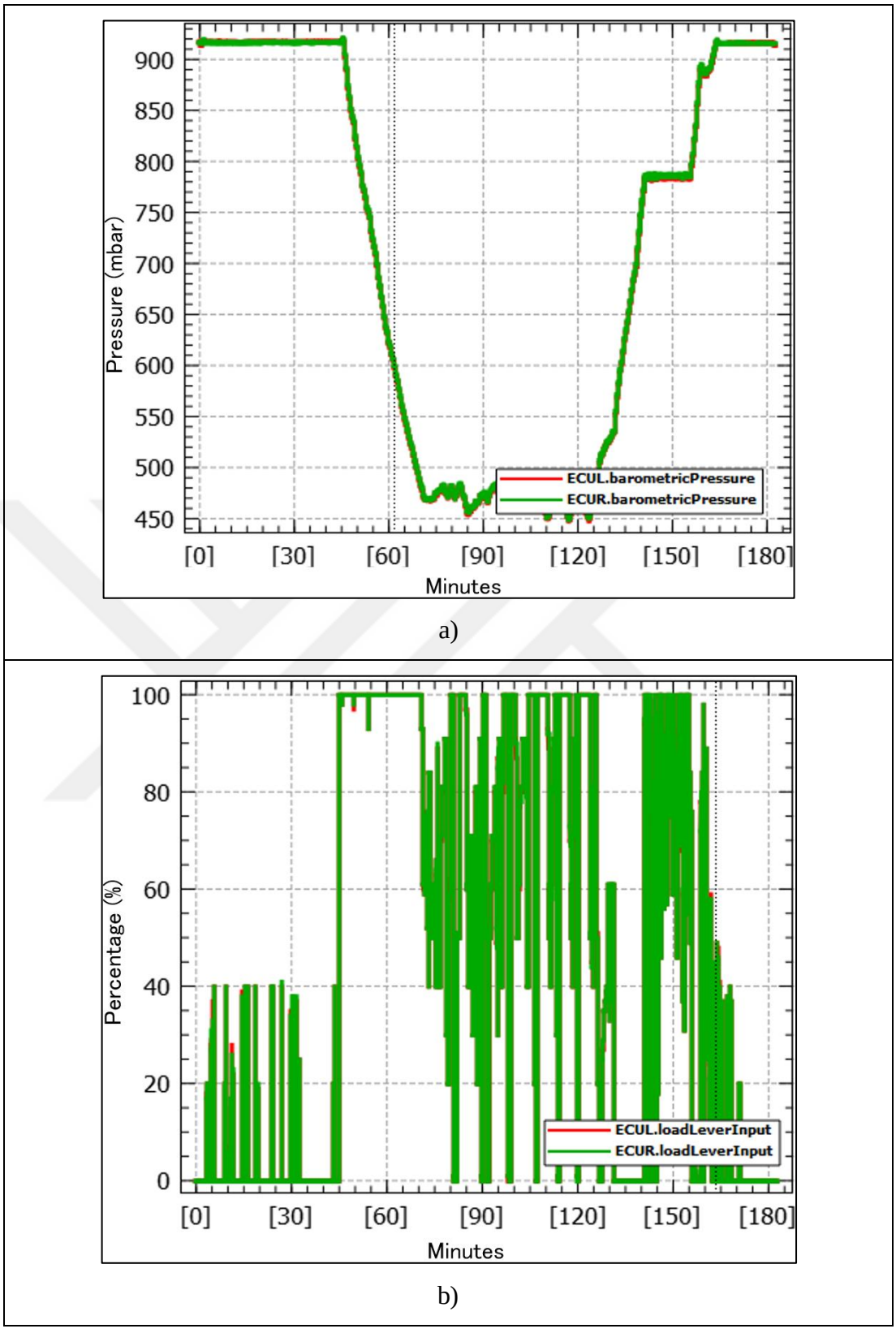

Figure 4.12: Auxiliary flight parameters a) barometric pressure b) load lever input (throttle position).

Figure 4.10 provides a trend of the manifold temperature. Upon closer scrutiny of the detailed data, it becomes evident that during the initial stages of take-off, the manifold temperature reaches its peak. Subsequently, as the aircraft continues its ascent and encounters cooler atmospheric conditions, the manifold temperature gradually decreases. This observed trend highlights the dynamic response of the cooling system to varying flight conditions. **Figure 4.13** shows detailed view of manifold temperature during take-off and at early phase of climbing.

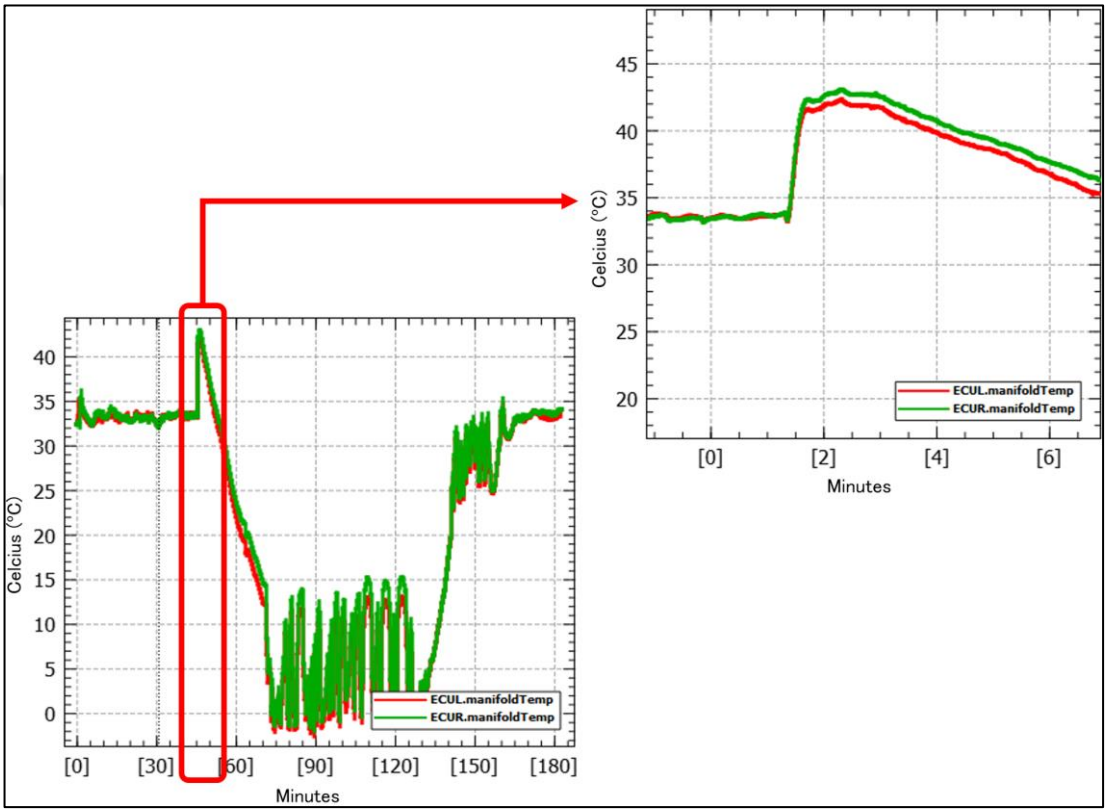

Figure 4.13: Manifold temperature at early phase of climbing and take-off.

Figure 4.11 shows that liquid cooling performance of engine. As it calculated from CFD results, heat successfully dissipated and temperatures doesn't exceed 100 ºC safe limit. Detailed view can be seen at **Figure 4.14**. Once again it is seen that most demanding condition with respect to heat rejection is early phase of climb.

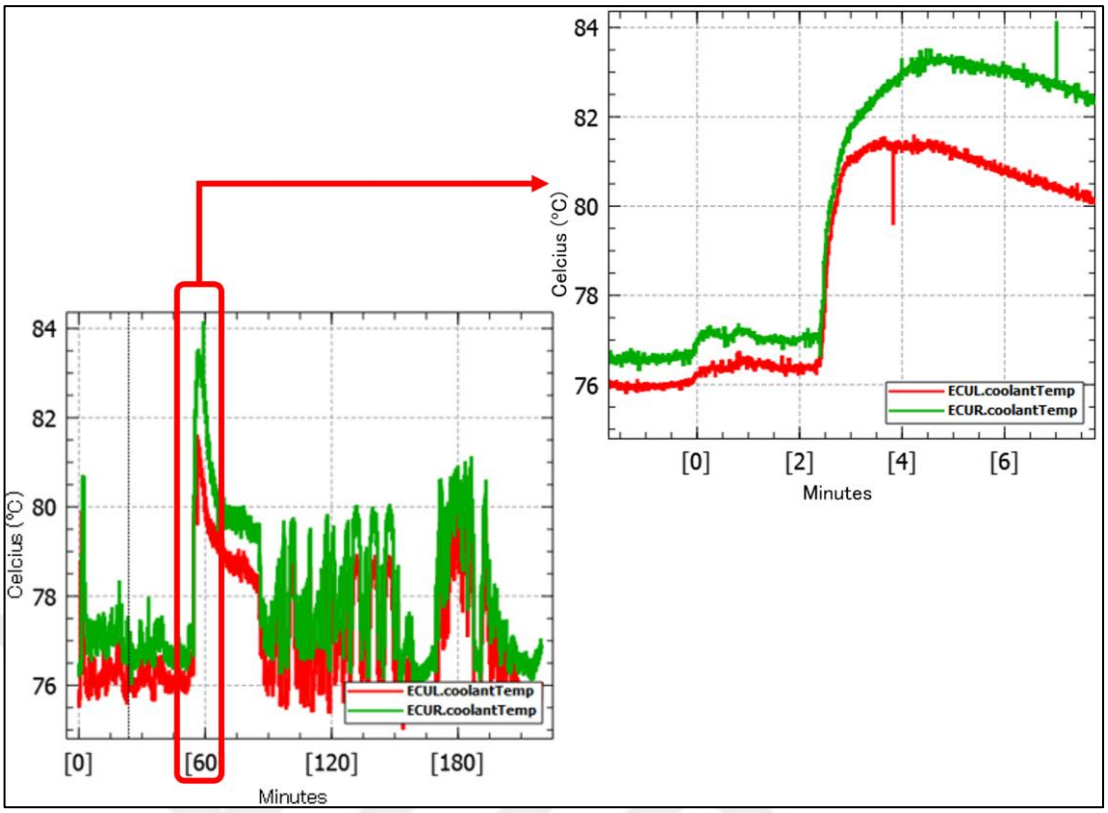

Figure 4.14 Coolant temperature at early phase of climbing and take-off.

Specifically, under an external temperature of 37 degrees Celsius, the duct design has been rigorously tested and confirmed to effectively fulfil the engine's cooling demands. This validation underscores the system's capability to maintain optimal operating temperatures even under challenging environmental conditions, thereby ensuring reliable engine performance throughout flight operations.

Computational fluid dynamics (CFD) analyses were utilized to determine the air duct option that provides the best performance in the cooling system design. Based on these analyses, the most optimal design was prototyped and subjected to test flights. During these test flights, the performance criteria specified in **Table 3.1**-**Table 3.3**, which include engine requirements, were evaluated. Detailed data obtained during flight is presented comprehensively in **Figure 4.5**-**Figure 4.12**.

This extensive dataset confirms that the air duct design created through computational fluid dynamics analysis successfully meets the cooling system requirements. This validation demonstrates that the design process effectively fulfils engineering requirements and positively impacts engine performance during flight.

5. CONCLUSION AND FUTURE WORK

This study focuses on designing air ducts for the radiator and intercooler of an aircraft equipped with a four-stroke engine featuring twin turbochargers. It also analyses their cooling performance prior to production using Computational Fluid Dynamics (CFD) software. Although the performance of air ducts can be measured in wind tunnels and during flight tests, these methods are expensive during the development phase. By utilizing CFD software as the design progresses towards its final configuration, the development budget can be optimized. Conducting multiple design analyses before production helps determine the optimal final design in a short time frame. For this purpose, three air ducts at each configuration have been designed to transfer the air mass flow rate required by the intercooler and radiator within the engine compartment to dissipate heat. The analysis results indicate that the designed air ducts meet the engine's cooling requirements. Flow separation regions caused by propeller effects are observed at the entrances of the air ducts, but these separations have not adversely impacted the overall performance of the intercoolers and radiators. Vortex generators could be used to manage airflow in stagnation areas formed by flow separations. Future work could enhance CFD models to incorporate real-world variables.

REFERENCES

[1] Çengel, Y. A., & Boles, M. A. (2015). “Thermodynamics: An Engineering Approach”, 8th Edition McGraw-Hill Education.

[2] Sparks W., https://slideplayer.com/slide/13819945/, (Date of Access: 10.02.2024).

[3] Web 1, (2023), https://tr.wikipedia.org/wiki/Cessna_172, (Date of Access: 22.03.2024).

[4] Web 2, (2023), https://tr.wikipedia.org/wiki/Piper_PA-28_Cherokee, (Date of Access: 22.03.2024).

[5] Web 3, (2024), https://en.wikipedia.org/wiki/Beechcraft_Bonanza, (Date of Access: 22.03.2024).

[6] Web 4, (2022), https://tr.wikipedia.org/wiki/Cirrus_SR22, (Date of Access: 22.03.2024).

[7] Web 5, (2024), https://en.wikipedia.org/wiki/Van%27s_Aircraft, (Date of Access: 22.03.2024).

[8] Web 6, (2024), https://tr.wikipedia.org/wiki/Focke-Wulf_Fw_190, (Date of Access: 22.03.2024).

[9] Purdy K. W., Christopher G., George C., Cromer O. C., https://www.britannica.com/technology/automobile, (Date of Access: 09.04.2024).

[10] Raorane S, (2017), “The development of method (tool) to model propeller propulsion models to be implemented in the potential flow simulation software 'Tornado' ”.

[11] Miley S. J., (1988), “Review of liquid-cooled aircraft engine installation aerodynamics”, J.Aircraft, 25 (3), 1-7.

[12] Piancastelli L., Cremonini M., Cassani S., Calzini F., Pezzuti E., (2018), “Intake and exhaust position optimization in the cooling duct of diesel helicopters”, ARPN Journal of Engineering and Applied Sciences, 13(17).

[13] Piancastelli L., Gatti A., Frizziero L., Ragazzi L., Cremonini M.,(2015), “CFD analysis of the Zimmerman's V173 STOL aircraft”, ARPN Journal of Engineering and Applied Sciences, 10(18), 8063-8070.

[14] Piancastelli L., Frizziero L., (2015), “Supercharging systems in small aircraft diesel common rail engines derived from the automotive field”, ARPN Journal of Engineering and Applied Sciences, 10(1), 20-26.

[15] Cassani S., (2017), “Airplane design: The superiority of FSW aluminium-alloy pure monocoque over CFRP "black" constructions”, ARPN Journal of Engineering and Applied Sciences, 12(2), 377-361.

[16] Pezzuti E., Valentini P. P., (2013), “Design and interactive simulation of cross-axis compliant pivot using dynamic spline”, International Journal on Interactive Design and Manufacturing, 7, 261-269.

[17] Valentini P. P., & Pezzuti E., (2016), “Computer-aided tolerance allocation of compliant ortho-planar spring mechanism”, International Journal of Computer Applications in Technology, 53, 369-374.

[18] El Ferik S., Omar H. M., Koesdwiady A. B., AL-Yazidi N. M., (2012), “OKID-based identification and control of unmanned ducted-fan helicopter”, IFAC Proceedings Volumes, 45(1), 115-120.

[19] Budiyono A., Wibowo S. S., (2007), “Optimal tracking controller design for a small scale helicopter”, Journal of Bionic Engineering, 4(4), 271-280.

[20] Cao Y., Yu Z., (2005), “Numerical simulation of turbulent flow around helicopter ducted tail rotor”, Aerospace Science and Technology, 9(4), 300-306.

[21] Chang S., Cho A., Choi S., Kang Y., Kim Y., Kim M., (2021), “Flight testing full conversion of a 40-kg-class tilt-duct unmanned aerial vehicle.”, Aerospace Science and Technology, 112, 106611.

[22] Cao C., Zhao G., Zhao Q., & Wang B., (2021), “Numerical investigation and optimization for interior duct shape of ducted tail rotor”, Aerospace Science and Technology, 115, 106778.

[23] Kothari V., Mehta Y., Shrivastav D., Panchal K., (2022), “Enhancement in the lift force of the Solid Fuel Ducted Ramjet (SFDR) with an increase in the controlling surface”, Materials Today: Proceedings, 50(5), 1878-1882.

[24] Naldi R., Macchelli A., Mimmo N., Marconi L., (2018), “Robust control of an aerial manipulator interacting with the environment”, IFAC-PapersOnLine, 51(13), 537-542.

[25] Invernizzi D., Lovera M., (2018), “Trajectory tracking control of thrust-vectoring UAVs”, Automatica, 95, 180-186.

[26] Manzoor T., Xia Y., Zhai D. H., Ma D., (2020), “Trajectory tracking control of a VTOL unmanned aerial vehicle using offset-free tracking MPC”, Chinese Journal of Aeronautics, 33(7), 2024-2042.

[27] Saeed A. S., Bani Younes A., Cai C., Cai G., (2018), “A survey of hybrid Unmanned Aerial Vehicles”, Progress in Aerospace Sciences, 98, 91-105.

[28] Marimuthu K., Umanath K., Krishnan S. J., (2021), “Investigating the conjugate heat transfer phenomena on various ducts for aircraft environmental control system”, Materials Today: Proceedings, 46(9), 3631-3638.

[29] Ritschl E., Theiner R., Hanus D., (2003), “Inlet Channel for a Ducted Fan Propulsion System of a Light Aircraft”.

[30] Weintraub D., Koppelberg J., Köhler J., Jeschke P., (2022), “Ducted fans for hybrid electric propulsion of small aircraft”, CEAS Aeronautical Journal, 13.

[31] Alexiou E., Dimitriou S., Dimopoulos T., Paliaikos D., Panagiotou P., Yakinthos K., (2021), “Cooling system design for the internal combustion engine of a BWB UAV prototype”, IOP Conference Series: Materials Science and Engineering, 1024(1).

[32] Zipszer G., Varró Sz., Darazs B., Gyöngyösi M., Horváth Á., (2022), “Artificial intelligent enhanced virtual blade model”, In Proceedings of the Conference on Modelling Fluid Flow (CMFF’22) (pp. CMFF22–029).

[33] Żółtak J., Stalewski W., (2014), “The Preliminary Design of the Air-Intake System and the Nacelle in the Small Aircraft-Engine Integration Process”, Aircraft Engineering and Aerospace Technology, 86(3), 250-258.

[34] Zipszer G., Darazs B., Horvath A., Toma D., Laki D., Gyöngyösi M., Suda J. M., Koren M., Farkas B., (2023), “CFD assessment of an ultralight aircraft including in-flight test data comparison”, Tech. Mech., 43(1), 189–202.

[35] Kuchemann D., Weber J., (1953), “Aerodynamics of Propulsion”, McGraw-Hill.

[36] Miley S. J., (1985), “Aerodynamics of liquid-cooled aircraft engine installations”, Presented at the General Aviation Aircraft Meeting and Exposition.

[37] Okumura K., (2000), “CFD Simulation by Automatically Generated Tetrahedral and Prismatic Cells for Engine Intake Duct and Coolant Flow in Three Days”, SAE Technical Paper 2000-01-0294.

[38] Furlan F., Chiereghin N., Kipouros T., Benini E., Savill M., (2014), “Computational design of S-Duct intakes for distributed propulsion”, Aircraft Engineering and Aerospace Technology, 86(6), 473-477.

[39] Mohler SR., “Wind-Us Flow Calculations For The M2129 S-Duct Using Structured And Unstructured Grids”, AIAA-2004-0525.

[40] Prasath G. S., Senthilkumar S., (2014), “CFD Study of Air Intake Duct”, International Journal of Engineering & Science Research, 4(5), 282–288.

[41] Versteeg H. K., Malalasekera W., (2007), “An introduction to computational fluid dynamics: The finite volume method”, 2nd edition, Pearson Education.

BIOGRAPHY

In 2019, Rifat Ramiz AYDIN received his degree in mechanical engineering from Hacettepe University. Since 2019, he has been employed at TAI as a propulsion systems design engineer.

PUBLICATION AND PRESENTATIONS FROM THE THESIS

Aydın R. R., Arslan M. A., (2024), "Duct Design of Reciprocating Engine Cooling System at Aircraft Which Has Tractor Configuration" , 3rd Bilsel International Ahlat Scientific Researches Congress, 900-909, Ahlat, Turkey, 8-9 June.